Superconductivity of strongly correlated systems / Supraconductivité des systèmes fortement corrélés

NMR studies on iron-pnictide superconductors: LaFeAs($O_{1-x}F_x$) and BaFe$_2$(As$_{1-x}$P$_x$)$_2$

Études par RMN des supraconducteurs pnictures à base de fer LaFeAs($O_{1-x}F_x$) et BaFe$_2$(As$_{1-x}$P$_x$)$_2$

Kenji Ishida [a,b,*], Yusuke Nakai [a,b], Shunsaku Kitagawa [a,b], Tetsuya Iye [a,b]

[a] Department of Physics, Graduate School of Science, Kyoto University, Kyoto 606-8502, Japan
[b] Transformative Research-project on Iron Pnictides (TRIP), Japan Science and Technology Agency (JST), Sanban-cho bldg., 5, Sanban-cho, Chiyoda, Tokyo 102-0075, Japan

A B S T R A C T

This review presents a summary of our NMR experiments on LaFeAs($O_{1-x}F_x$) and BaFe$_2$(As$_{1-x}$P$_x$)$_2$. The authors introduce the key NMR experimental results which reveal their physical properties in the normal and superconducting states. From the comparison of the NMR results between the two systems, we point out that the superconducting gap structure and the relationship between superconductivity and magnetic fluctuations probed with NMR are quite different between the two systems.

© 2011 Académie des sciences. Published by Elsevier Masson SAS. All rights reserved.

R É S U M É

Cet article de revue couvre nos résultats obtenus par RMN sur les supraconducteurs pnictures à base de fer LaFeAs($O_{1-x}F_x$) et BaFe$_2$(As$_{1-x}$P$_x$)$_2$. Nous introduisons les mesures clefs qui ont sondé leurs propriétés tant normales que supraconductrices. La comparaison des deux systèmes montre que la structure du gap supraconducteur ainsi que la relation entre supraconductivité et fluctuations magnétiques, telles que vue par la RMN, sont très différentes dans les deux cas.

© 2011 Académie des sciences. Published by Elsevier Masson SAS. All rights reserved.

1. Introduction

The discovery of iron-oxypnictide superconductor LaFeAs($O_{1-x}F_x$) with $T_c = 26$ K [1] surprised physicists and chemists studying superconductivity all over the world. This is because Fe metal is a ferromagnet and the Fe site is thought to play an important role for such an unexpectedly high T_c. Shortly after this discovery, application of pressure increases T_c in LaFeAs($O_{1-x}F_x$) even further to 43 K [2], and the replacement of the nonmagnetic La by magnetic rare earth elements enhances T_c up to 56.3 K, which is the current record of the iron-pnictide superconductor [3–6]. This extraordinary high T_c attained by iron-based superconductors has demonstrated that high-T_c superconductivity is more general than previously thought. It is quite important to investigate physical properties of the iron-pnictide superconductivity in order to understand the mechanism of high-T_c superconductivity.

---

* Corresponding author at: Department of Physics, Graduate School of Science, Kyoto University, Kyoto 606-8502, Japan.
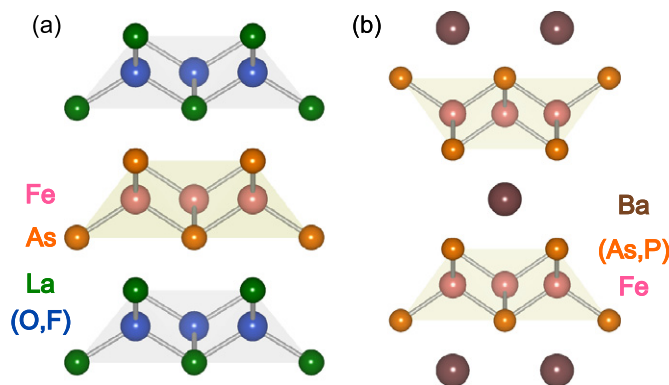*E-mail address:* kishida@scphys.kyoto-u.ac.jp (K. Ishida).

Fig. 1. Crystal structures (a) LaFeAsO (refereed to as "1111" in the article) and (b) BaFe$_2$As$_2$ ("122").

We have studied normal and superconducting (SC)-state properties on two iron-pnictide systems; LaFeAs(O$_{1-x}$F$_x$) with the "1111" structure [7–9] and BaFe$_2$(As$_{1-x}$P$_x$)$_2$ with the "122" structure [10,11]. Their crystal structures are shown in Fig. 1.

Superconductivity in the two systems appears upon F- or P-doping in close proximity to parent phases which exhibit stripe-type antiferromagnetic (AFM) order, along with structural distortion from tetragonal to orthorhombic phases [12,13,7]. Then it is natural to inquire an interplay between superconductivity and spin fluctuations associated with the magnetic ordering. In addition, since electron–phonon coupling is too weak to account for the high T_c [14], it has been invoked that the spin fluctuations due to nesting between the disconnected Fermi surfaces (FSs) are the source of the pairing interaction [15–17]. We consider that investigations on doping dependence of the normal and SC state properties will provide crucial information concerning the relationship between superconductivity and spin fluctuations in the iron-pnictide superconductor.

In this article, we review our NMR studies on LaFeAs(O$_{1-x}$F$_x$) and BaFe$_2$(As$_{1-x}$P$_x$)$_2$, which have been performed to investigate systematic evolution of spin fluctuations in the two systems. Our NMR results show that the SC gap structure and the relationship between superconductivity and spin fluctuations probed by NMR measurements are quite different between LaFeAs(O$_{1-x}$F$_x$) and BaFe$_2$(As$_{1-x}$P$_x$)$_2$, although superconductivity emerges in the similar situation.

2. Experimental results

2.1. NMR in LaFeAs(O$_{1-x}$F$_x$) [7–9]

Superconductivity in LaFeAs(O$_{1-x}$F$_x$) emerges at around $x = 0.04$. The F-doping, corresponding to electron doping, suppresses the nesting between hole and electron pocket FSs and would alter the low-lying excitations originating from the nesting-related magnetic fluctuations. We performed systematic studies on LaFeAs(O$_{1-x}$F$_x$) through ^{75}As and ^{139}La NMR in a wider F-doping range in order to understand the entire nature of the spin dynamics upon F-doping.

Polycrystalline samples of LaFeAs(O$_{1-x}$F$_x$) ($x = 0.0$, 0.04, 0.07, 0.11, 0.14) synthesized by solid-state reactions [1] were ground into a powder for the NMR measurements. All the samples were examined using powder X-ray diffraction (XRD; Bruker D8 Advance TXS) with Cu Kα radiation, indicating that all the samples are mostly composed of a single phase. The contents of the dopant (x) were determined from lattice constants using Vegard's volume rule [18]. Electrical resistivity (ρ) measurements were performed using a usual four-probe technique, and the temperature dependence of ρ in these samples is shown in Fig. 2. The T_c's determined from the zero-resistivity are 16.3, 22.5, 22.5, 12.5 K for $x = 0.04$, 0.07, 0.11, 0.14, and the T_c determined by the onset of the Meissner signal are 17.5, 22.5 and 22.7 K for $x = 0.04$, 0.07 and 0.11, respectively. Two independent measurements reasonably coincide with each other.

2.1.1. Undoped LaFeAsO

Fig. 3 shows ^{139}La ($I = 7/2$)-NMR spectra for undoped LaFeAsO obtained by sweeping an external field at a fixed frequency 15.35 MHz. In general, when an electric field gradient is present at the La site, a La NMR spectrum consists of seven peaks arising from ($m \leftrightarrow m - 1$) ($m = 7/2, 5/2, \ldots$ and $-5/2$) transitions due to the electric-quadrupole interaction [19]. However, a quite different ^{139}La NMR spectrum is observed in the undoped LaFeAsO at 10 K; the central peak arising from the $1/2 \leftrightarrow -1/2$ transition is split due to internal magnetic field at the La site. With increasing temperature, the splitting of the NMR spectrum denoted by the two red arrows in Fig. 3 decreases gradually and typical powder-pattern spectra consisting of seven transitions were observed above 150 K. The observed spectrum for the undoped LaFeAsO suggests an antiferromagnetic ordering below ~ 150 K, which is consistent with an anomaly of the electrical resistivity and susceptibility around 150 K [1]. Similar temperature variation of the ^{139}La-NMR spectra in LaFeAsO was also observed by Mukuda et al. [20]. The ^{139}La NMR spectrum clearly indicates that the undoped LaFeAsO is in a magnetically ordered state below ~ 150 K.
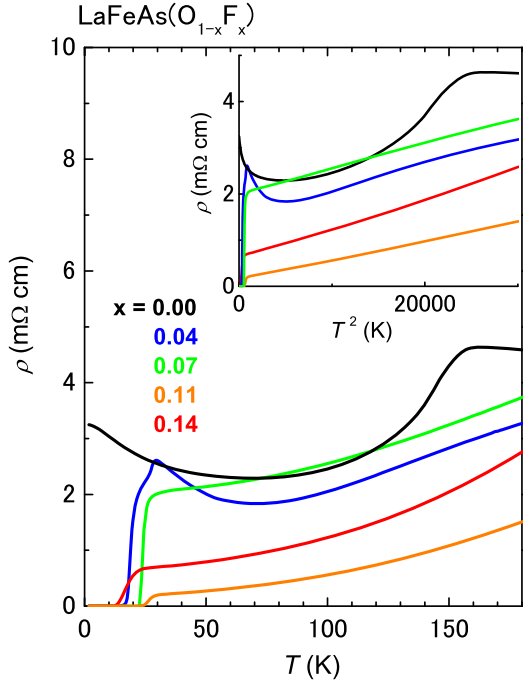
Fig. 2. The temperature dependence of resistivity ρ in LaFeAs(O$_{1-x}$F$_x$) [8]. The insert is the plot of ρ against T^2. Copyright 2009, the IOP Publishing Ltd.
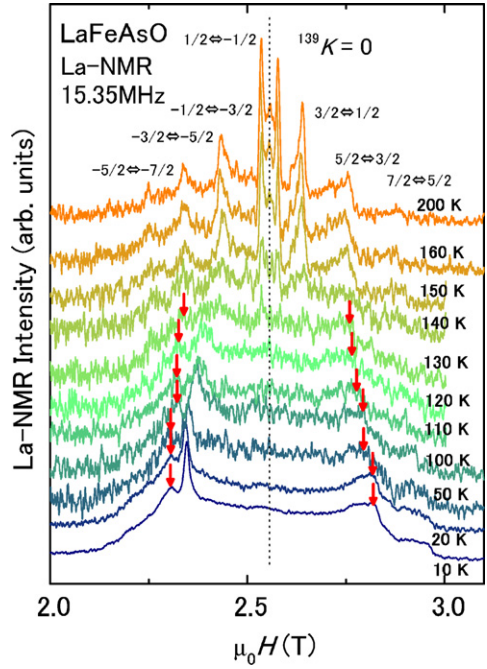

Fig. 3. Field-sweep ^{139}La-NMR spectra at a series of temperatures through $T_N \sim 142$ K in undoped LaFeAsO [8]. The spectra have been offset vertically. The arrows indicate the fields at which we measured the internal magnetic field. (For interpretation of the references to color in this figure, the reader is referred to the web version of this article.) Copyright 2009, the IOP Publishing Ltd.
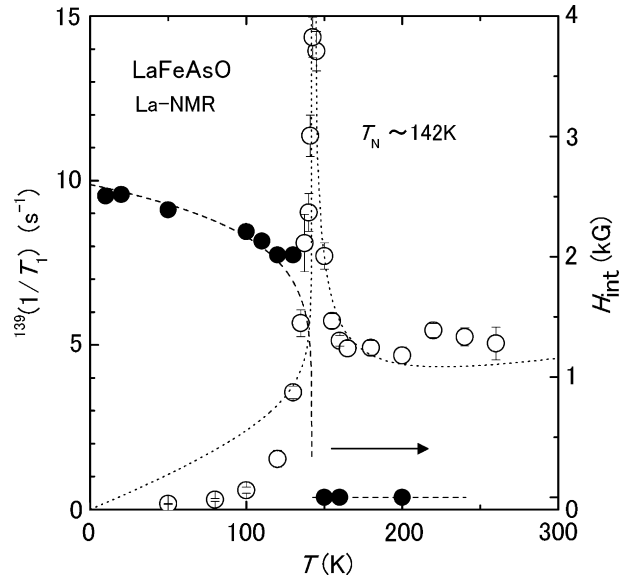

Fig. 4. T-dependence of $1/T_1$ of ^{139}La ($\bigcirc$) and the internal magnetic field ($\bullet$) of undoped LaFeAsO ($x = 0$) [8]. The dotted line is a fit to the SCR theory for weak itinerant antiferromagnets (see text). Copyright 2009, the IOP Publishing Ltd.

The internal field at the La site arises from the hyperfine field from adjacent Fe atoms, and is related with the Fe ordered moments. The internal field H_{int} determined from the half width of the splitting is shown in Fig. 4 (filled circles). From the As-NMR study on single-crystal BaFe$_2$As$_2$ shown later, it was revealed that the c-axis internal field arises at the As site in the ordered state with the stripe-type magnetic structure [21,22] suggested from the neutron-scattering measurement [12]. Thus, the direction of H_{int} is considered to be the c-axis, since the La site is the same geometrical configuration as the As site with respect to the magnetic Fe site. The dashed line in Fig. 4 is a fitting to the following
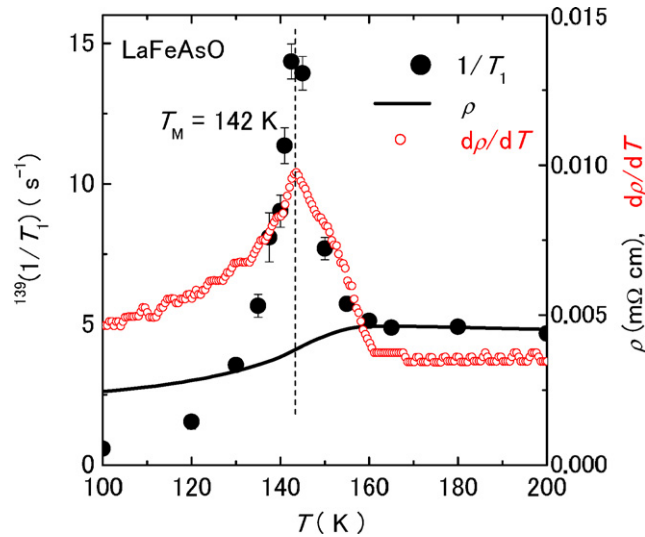
Fig. 5. T-dependence of $1/T_1$ of ^{139}La, resistivity (ρ) and T derivative of ρ ($d\rho/dT$) in LaFeAsO in the T range of 100–200 K [8]. Copyright 2009, the IOP Publishing Ltd.

expression, $M(T)/M_0 = [1 - (T/T_N)]^{0.15}$. The growth of $M(T)/M_0$ below T_N is much steeper than the 3D mean field value (0.5), and the transition to the antiferromagnetic state is almost first-order like. We consider that two-dimensionality of magnetic fluctuations is also responsible for the reduced value of the critical exponent, since similar rapid growth was actually reported in the cuprate antiferromagnet La_2CuO_4 with a critical exponent $\beta \sim 0.1$ [23], which possesses magnetic fluctuations with 2D nature.

Further insight into the magnetic properties in the undoped LaFeAsO is obtained from $1/T_1$ measurements. Fig. 4 shows the temperature dependence of $1/T_1$ of ^{139}La, which was measured at $H = 2.54$ T in the ^{139}La NMR spectrum. $1/T_1$ exhibits a divergence at $T_N = 142$ K, and the overall temperature dependence of $1/T_1$ in Fig. 4 is fitted to the SCR theory for weak itinerant antiferromagnets [24]:

$$\frac{1}{T_1} = \begin{cases} aT + bT/\sqrt{T - T_N}, & T > T_N \\ cT/M(T), & T < T_N \end{cases} \tag{1}$$

where $a = 0.005$ s^{-1} K^{-1}, $b = 0.13$ s^{-1} K$^{-1/2}$ and $c/M_0 = 0.02$ s^{-1} K^{-1} are fitting parameters, and $M(T) = M_0(1 - T/T_N)^{0.15}$ is an antiferromagnetic order parameter as mentioned above. The first term in (1) comes from usual Korringa relaxation expected in a metal. It is noteworthy that $1/T_1$ related to the q-averaged dynamical susceptibility shows a divergence at 142 K whereas a clear anomaly is not observed in the static susceptibility. These are the characteristic features of an itinerant antiferromagnet observed in V_3Se_4, in which the ordered **q**-vector is far from **q** = 0 [25].

Although the SCR expression roughly captures the behavior of $1/T_1$ in the undoped LaFeAsO, the sharp decrease of $1/T_1$ below T_N cannot be reproduced by the expression. The discontinuous decrease of $1/T_1$ and abrupt increase of H_{int} was observed in single-crystal $BaFe_2As_2$ and $CaFe_2As_2$ [21,22,26] in which the structural and magnetic transitions occurs simultaneously with a first-order character. Therefore, the sharp decrease of $1/T_1$ and abrupt increase of H_{int} below T_N also suggest the magnetic transition in LaFeAsO possesses a first-order-like character, although a hysteresis behavior at about the magnetic transition was not reported. It should be noted that the divergence of $1/T_1$ is affected by a structural phase transition from the tetragonal ($P4/nmm$) to orthorhombic ($Cmma$) occurring at 165 K upon cooling, which was observed by synchrotron X-ray diffraction in the same batch sample as ours [13]. In fact, as shown in Fig. 5, $1/T_1$ starts to increase just below 160 K, where the resistivity shows a kink due to this structural transition. It was found that the temperature derivative of the resistivity shows a sharp peak at T_N determined by the peak of $1/T_1$. The $1/T_1$ result indicates that a characteristic frequency of the magnetic fluctuations start to decrease below 160 K where the structural transition occurs, and becomes static below 142 K. The relationship between the structural and magnetic transition suggests the importance of the spin Jahn–Teller effect in LaFeAsO, where the direction of the ordered moments is determined due to the crystal distortion. To understand the origin of magnetic ordering, it is desired to investigate the relationship between the structural transition temperature and T_N with the same technique in various samples.

The present ^{139}La NMR results are in good agreement with the neutron-scattering results [12]. The neutron-scattering measurements revealed a small ordered moment $0.37\mu_B$/Fe with the stripe-type magnetic structure **Q** = $(\pi, 0), (0, \pi)$ in the "*unfolded*" Brillouin zone in the undoped LaFeAsO below 134 K, which is slightly lower than the lattice anomalous temperature 155 K.
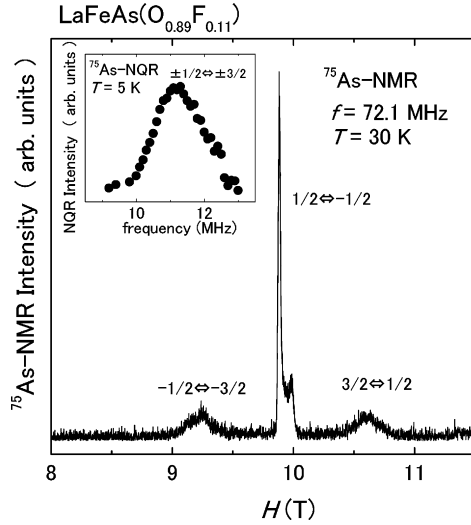
Fig. 6. Field-swept ^{75}As-NMR spectrum of powdered LaFeAs(O$_{0.89}$F$_{0.11}$) obtained with a fixed frequency $f = 72.1$ MHz and at 30 K [8]. The insert shows the ^{75}As-NQR spectrum obtained by sweeping frequency at 5 K. Copyright 2009, the IOP Publishing Ltd.
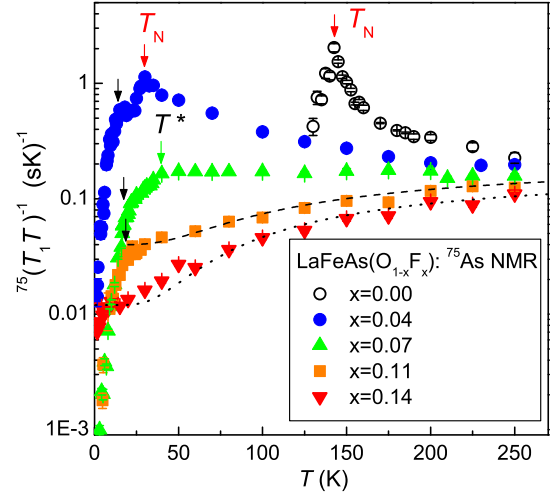
Fig. 7. Doping dependence of ^{75}As $1/T_1T$ [8]. The black (green) arrows denote T_c (T^*) (see text). The broken (dotted) line is a fitting to the data for $x = 0.11$ (0.14). The red arrows indicate T_N.

2.2. ^{75}As NMR in the normal state of LaFeAs(O$_{1-x}$F$_x$)

We move to ^{75}As ($I = 3/2$) NMR results on the SC compounds. $1/T_1$ of ^{75}As was obtained by fitting the time dependence of the magnetization recovery after a saturation pulse at the intense peak of the central ($1/2 \Leftrightarrow -1/2$) transition (corresponding to $H_\parallel$ the ab-plane) in $H \simeq 9.89$ T at a fixed frequency 72.1 MHz (see Fig. 6) [7]. A systematic doping evolution of spin dynamics in the normal state is observed in the T-dependence of $1/T_1T$ at the As site in LaFeAs(O$_{1-x}$F$_x$) as shown in Fig. 7. Similar results were also reported by Nakano et al. [27]. In undoped LaFeAsO, a clear critical slowing down due to the AFM ordering with $\mathbf{q}_{\text{stripe}}$ is observed at 142 K. For $x = 0.04$, $1/T_1T$, which is the sum of low-lying dynamical susceptibility $\chi(\mathbf{q})$ over the Brillouin zone, follows a Curie–Weiss temperature dependence down to 30 K. In contrast, the magnetic susceptibility $\chi(\mathbf{q} = 0)$ of LaFeAs(O$_{1-x}$F$_x$) decreases with decreasing temperature [28]. Their contrasting behavior is a clear indication of the development of AFM fluctuations away from $\mathbf{q} = 0$ at $x = 0.04$. At $x = 0.07$, $1/T_1T$ remains nearly constant down to $T^* \simeq 40$ K, then decreases rapidly. T^* can be ascribed neither to a magnetic anomaly nor to an SC transition; invariant ^{75}As-NMR spectra rules out the former, and the absence of Meissner signal excludes the latter. The reduction of $1/T_1T$ below T^*, approximately 20 K higher than T_c, is reminiscent of the pseudogap behavior observed in the cuprates [29]. The pseudogap-like behavior is more pronounced for $x = 0.11$ and 0.14, where $1/T_1T$ decreases on cooling, approaching nearly constant values, as shown in Fig. 8. By fitting the data to $1/T_1T = a + b\exp(-\Delta_{\text{PG}}/T)$, we obtained $a = 0.04$ (s^{-1} K^{-1}), $b = 0.19$ (s^{-1} K^{-1}) and $\Delta_{\text{PG}} = 172 \pm 12$ K for $x = 0.11$, and $a = 0.012$ (s^{-1} K^{-1}), $b = 0.18$ (s^{-1} K^{-1}) and $\Delta_{\text{PG}} = 165 \pm 15$ K for $x = 0.14$, yielding almost the same pseudogap energies Δ_{PG} for $x = 0.11$ and 0.14 within experimental uncertainty. On the basis of our present results along with those reported previously, we generate the phase diagram for LaFeAs(O$_{1-x}$F$_x$) shown in Fig. 9. The doping dependence of $1/T_1T$ indicates that the nature of the pseudogap in LaFeAs(O$_{1-x}$F$_x$) and the cuprates differs significantly: (1) In the cuprates, $1/T_1T$ decreases from temperatures well above T_c and no clear anomaly is observed at T_c. In contrast, a clear anomaly in $1/T_1T$ is found at T_c for $x = 0.11$, and Korringa behavior ($T_1T = $ const.), suggestive of a Fermi-liquid (FL) state, is observed at low temperatures, which may be related to the T^2 behavior of the resistivity. Considering the multi-band nature of LaFeAs(O$_{1-x}$F$_x$) and electron doping, these results suggest that the hole FS sheets exhibit pseudogap behavior while others contribute to the FL state. (2) The pseudogap behavior in LaFeAs(O$_{1-x}$F$_x$) becomes more pronounced with F-doping, opposite to the behavior observed in the cuprates. There, the pseudogap behavior is most pronounced near the AFM phase boundary, and it is most likely that AFM correlations may be responsible for the pseudogap behavior. In LaFeAs(O$_{1-x}$F$_x$), however, low-energy AFM correlations are unlikely to yield the pseudogap behavior since no apparent AFM fluctuations are observed via ^{75}As NMR for $x = 0.11$ and 0.14. Furthermore, almost the same Δ_{PG} is observed through ^{57}Fe-NMR measurements, suggesting that the pseudogap does not have $\mathbf{q}$-dependence [32]. From the theoretical point of view, Ikeda suggested that the pseudogap behavior in $1/T_1T$ may originate from band structure effects near Fermi energy [33]. The existence of a high density of states (DOS) just below the Fermi level, which is assigned to a hole FS around Γ' consisting of $d_{x^2-y^2}$ orbitals in the *unfolded* Brillouin zone, gives rise to a T-dependent DOS, and the calculated T-dependence of $1/T_1T$ is consistent with our results. Thus, the pseudogap behavior originates from its characteristic band structure in LaFeAs(O$_{1-x}$F$_x$).
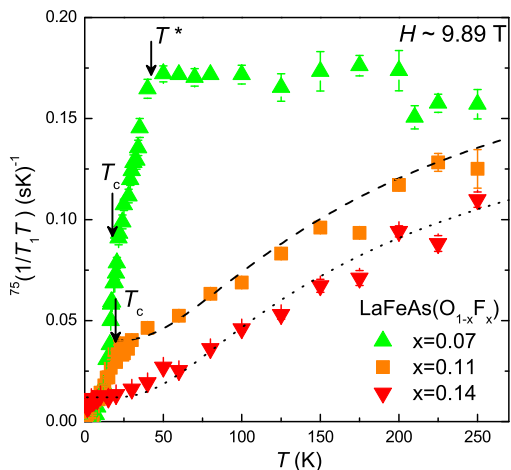
Fig. 8. T-dependence of $1/T_1T$ of ^{75}As at $x = 0.07$, 0.11, and 0.14 [8]. The broken (dotted) line is a fitting to $1/T_1T$ of ^{75}As for $x = 0.11$ ($x = 0.14$) (see text). Copyright 2009, the IOP Publishing Ltd.
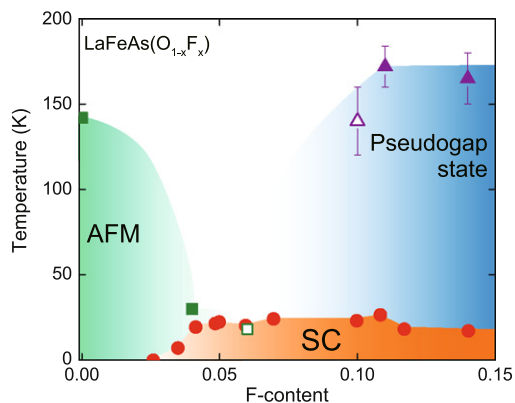

Fig. 9. Phase diagram of LaFeAs(O$_{1-x}$F$_x$) [8]. The closed (open) triangle designates the pseudogap energy determined from $1/T_1$ of ^{75}As (Knight shift of ^{19}F cited from Ref. [30]). The blue triangle indicates T^* below which the pseudogap behavior was observed. The closed square indicates the magnetic ordering temperature T_N determined from ^{139}La and ^{75}As NMR. The open square indicates the onset temperature of spin-glass-like magnetism determined from μSR. [31] T_c (closed circle) is determined from the temperature where ρ becomes half as that at the onset temperature [1]. (For interpretation of the references to color in this figure, the reader is referred to the web version of this article.) Copyright 2009, the IOP Publishing Ltd.
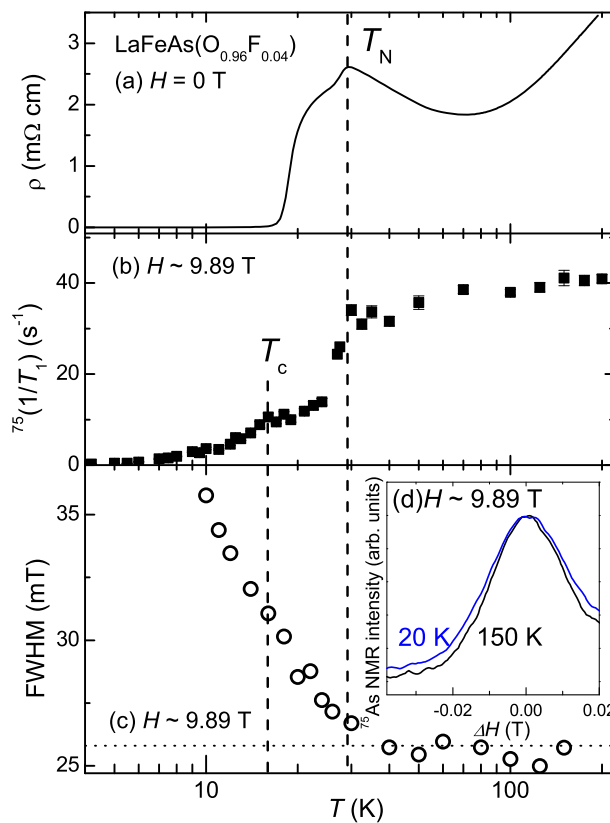

Fig. 10. T-dependence of (a) resistivity, (b) $1/T_1$ of ^{75}As, (c) the FWHM of the ^{75}As NMR spectra and (d) ^{75}As-NMR spectrum where $H_\parallel$ the ab-plane in LaFeAs(O$_{0.96}$F$_{0.04}$). The spectrum at 20 K is shifted to be conformed to the spectral peak at 150 K.

2.2.1. ^{75}As NMR in the superconducting state of LaFeAs(O$_{1-x}$F$_x$)

Next, we discuss the F-doping evolution of SC features in LaFeAs(O$_{1-x}$F$_x$). The $x = 0.04$ sample (LaFeAs(O$_{0.96}$F$_{0.04}$)) locates near the boundary between the AFM and SC phases, which would help us elucidate an interplay between magnetism and superconductivity in LaFeAs(O$_{1-x}$F$_x$). Fig. 10 displays the T-dependence of resistivity ρ, $1/T_1$ of ^{75}As, the full width
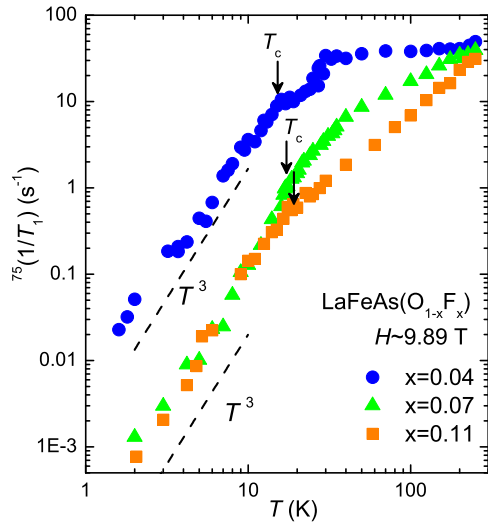
Fig. 11. T-dependence of $1/T_1$ of ^{75}As measured at the peak corresponding to $H_\parallel$ the ab-plane [8]. Copyright 2009, the IOP Publishing Ltd.
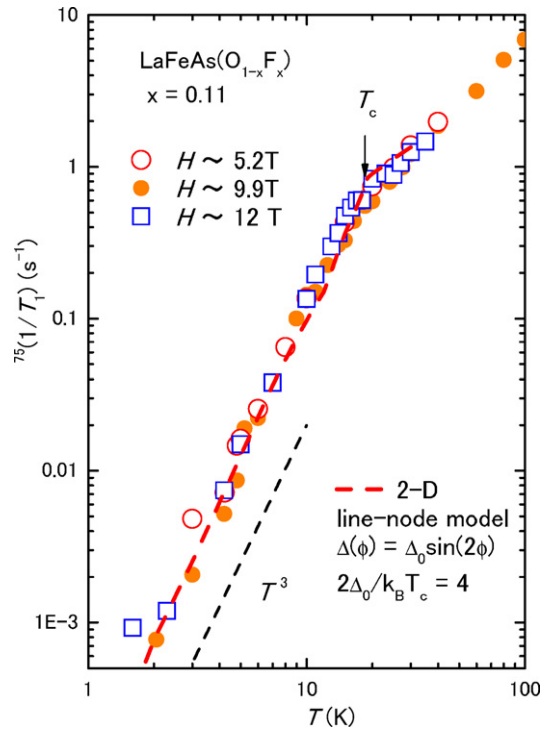

Fig. 12. T-dependence of $1/T_1$ of ^{75}As in LaFeAs($O_{0.89}F_{0.11}$) under 5.2, 9.9 and 12 T [8]. The dashed curve is a calculation with assuming a line node gap $\Delta(\phi) = \Delta_0 \sin(2\phi)$ with $\Delta_0 = 2k_B T_c$. Copyright 2009, the IOP Publishing Ltd.

at half maximum (FWHM) of the ^{75}As-NMR spectra at $x = 0.04$. Fig. 2 indicates that the resistivity of $x \geqslant 0.07$ samples exhibits a metallic behavior ($\rho \propto T^2$ holds below 150 K), but that at $x = 0.04$, it exhibits a nonmetallic behavior below 70 K. ρ at $x = 0.04$ starts to increase with lowering temperature, and then drops below 30 K (Fig. 10 (a)). $1/T_1$ is determined with a single component above 30 K, and the T-dependence of $1/T_1 T$ follows the Curie–Weiss law $1/T_1 T \propto 1/(T + \theta)$ with $\theta = 10.3 \pm 2$ K between 30 K and 200 K [7], which is a characteristic features of the development of AFM fluctuations. Below 30 K, a short T_1 component appears, and the longer T_1 component that exhibits a superconducting anomaly at T_c is plotted in Fig. 10(b); $1/T_1$ decreases suddenly below 30 K and then exhibits superconductivity below $T_c \simeq 16$ K. This anomaly at 30 K cannot be ascribed to the occurrence of superconductivity because ac susceptibility does not exhibit any anomaly near 30 K. Instead, this is attributed to a weak magnetic ordering, because the line width increases gradually below 30 K (Fig. 10(c), (d)). The ordered moment is very small because the broadening of the ^{75}As and ^{139}La NMR spectra is much smaller than that of the undoped LaFeAsO [7,20]. A divergence of $1/T_1$ was observed at $T_N \simeq 142$ K in LaFeAsO due to the occurrence of the AFM ordering. In contrast, we did not find such a huge increase of $1/T_1$ but just a decrease of $1/T_1$, indicating that the magnetic anomaly becomes weakened upon F-doping. As noted above, there emerges a short component of $1/T_1$ below 30 K whose value is approximately 65% at 3 K. Since it is difficult to attribute such a large amount to inhomogeneous F-concentration, this distribution of $1/T_1$ implies a phase separation into the magnetically ordered and SC phases. Indeed, recent μSR measurements suggest the presence of a phase separation into SC and spin-glass-like magnetic phases in LaFeAs($O_{0.94}F_{0.06}$) near the phase boundary [31]. Our $x = 0.04$ result is consistent with this μSR experiment. It is considered that there exist AFM and SC regions and thus phase separation occurs in underdoped LaFeAs($O_{1-x}F_x$).

Next, we discuss the SC-gap properties from the T-dependence of $1/T_1$ in the SC state. Fig. 11 shows the T-dependence of $1/T_1$ of ^{75}As for $x = 0.04$, 0.07 and 0.11, which was measured in $H \sim 9.9$ T. As mentioned above, a short component of T_1 appears gradually in all samples below 30 K and its fraction increases with decreasing T. The appearance of the short component of T_1 is considered to be due to a tiny amount of a spin-glass-like magnetic region. However, the fraction of the longer component of T_1 is dominant even at low temperatures, and thus the longer component is shown in Fig. 11.

It was found that $1/T_1$ at $x = 0.04$, 0.07, and 0.11 decreases suddenly without showing a Hebel–Slichter (coherence) peak just below T_c, and that the T^3 dependence of $1/T_1$ was observed in the SC state for all samples. Although the absence of the coherence peak and T^3 dependence observed in $1/T_1$ strongly suggest the presence of the linenodes, various experimental results are inconsistent with the presence of the linenodes. It is known in anisotropic superconductors with nodes that an applied magnetic field induces the extra relaxation rate originating from the Volvik effect [34]. It was pointed out that the quasiparticle states are extended outside the vortex cores with ungaped spectrum in a d-wave superconductor, which gives rise to a field-induced relaxation rate. However, such field-induced relaxation rate was not observed in

LaFeAs(O$_{1-x}$F$_x$) as shown in Fig. 12. It was found that the T^3 behavior holds down to 4 K ($\sim 0.2T_c$) in the field range of 5.2–12 T within the experimental error (typically $\Delta T_1 \sim 10\%$), indicative of the absence of the field-induced $1/T_1$. We also point out that a residual density of states (DOS) suggested from the low-temperature Korringa behavior was not observed in the $x = 0.04$, 0.07 and 0.11 samples. In non-s-wave superconductors with line nodes, it is well known that the residual DOS is easily induced by a tiny amount of impurities and crystal imperfections, and was observed in most of unconventional superconductors [35,36]. It seems that the absence of the residual DOS is contrary to non s-wave models, since the LaFeAs(O$_{1-x}$F$_x$) is considered to possess the randomness related to the F substitution. Furthermore, various experimental results, such as penetration-depth and photo-emission measurements in the FeAs superconductors, suggest the presence of a finite superconducting gap, which is inconsistent with the our NMR results [37,38].

To reconcile with these experimental results, the $s_\pm$ state with the anisotropic gap are considered as a most promising state in the FeAs superconductors at present. In this state, the superconducting gap is sign reverse between hole and electron FSs across the nesting vector. In a case of the anisotropic s-wave gap ($\Delta(\phi) = |\Delta_0 \sin(2\phi)|$ [39]) and s_{++}-wave gap, a coherence peak remains since the coherence factor does not vanish when the gap function is integrated over the FSs. However, the resistivity follows a T^2 dependence in a wide temperature range between T_c and 150 K in $x = 0.07$ and 0.11; it is hard to consider that the quasiparticle damping suppresses the coherent peak just below T_c.

Alternatively, the absence of the coherence peak is consistently understood by the sign-changed superconducting gaps realized in the $s_\pm$ state [40–42]. Furthermore, it was reported that the T^3 dependence in the superconducting state can be reproduced with the $s_\pm$ state with an anisotropic character of the superconducting gap at the electronic FSs together with some impurity effect [43]. However, since the exponential temperature dependence of $1/T_1$ should be observed in a impurity-free sample with the $s_\pm$ pairing, further NMR measurements using high-quality samples are important, in particular, $1/T_1$ measurements at low temperatures are crucial.

We point out that the T^3 dependence is observed even in the $x = 0.04$ sample located in the boundary of two phases. This behavior is in contrast to that of the superconductors which coexist with magnetism such as the pressure-induced heavy-fermion superconductor CeRhIn$_5$ [44]. In CeRhIn$_5$ near the critical pressure, although $1/T_1$ decreases sharply just below T_c, $1/T_1$ becomes proportional to T far below T_c. It is reported that the $1/T_1 \propto T$ behavior does not originate from residual density of states (DOS) but from the gapless nature in the low-lying excitation due to the microscopic coexistence of antiferromagnetism and superconductivity in CeRhIn$_5$ [44]. The different behaviors of $1/T_1$ suggest that the nature of coexistence is different for the two superconductors. In addition to the emergence of a short component of $1/T_1$ below T_N as discussed above, the robust T^3 dependence of $1/T_1$ at $x = 0.04$ also supports a phase separation into the magnetically ordered and SC phases because the magnetic ordering would affect the T^3 behavior if the magnetic order and superconductivity coexist microscopically.

Here, we discuss the relationship between magnetic fluctuations and superconductivity. Since the electron–phonon coupling was shown to be too weak to account for the high T_c of the iron-oxypnictide superconductors [14,45], spin fluctuation is one of the plausible candidates for the pairing interaction [15–17]. Due to the disconnected FSs in the iron oxypnictide, nesting-related spin fluctuations would be the origin of the pairing interaction. F-doping (corresponding to electron doping) is likely to enhance a mismatch between the FSs, leading to the suppression of the spin fluctuations. This is actually observed in the present NMR study; the significant antiferromagnetic fluctuations in $x = 0.04$ are suppressed in $x = 0.07$. It should be noted that $1/T_1$ in the SC state of $x = 0.07$ is identical to that in $x = 0.11$, although $1/T_1$ in the normal state is different with each other. An almost constant value of T_c against the F concentration, irrelevant to the drastic change of $1/T_1T$ in the normal state, suggests that the spin fluctuations observed through the $1/T_1$ measurements do not play a vital role for the superconductivity. However, it should be noted that the $1/T_1$ measurements can detect the low-energy magnetic fluctuations (typically $\sim$ mK order), and might fail to detect important magnetic fluctuations if their characteristic energy exceeds the limitation of the NMR experiments. Therefore, the inelastic neutron experiments over a wide q-space and energy range are needed for uncovering magnetic fluctuations thoroughly, and are important for clarifying the relationship between the superconductivity and magnetic fluctuations.

2.3. NMR study in the 122 system

Superconductivity in AFe$_2$As$_2$ ($A = $ Ba, Sr and Ca) with the "122" structure appears where antiferromagnetism is suppressed via chemical substitution or pressure. The well-known systems are (Ba$_{1-x}$K$_x$)Fe$_2$As$_2$ [46] and Ba(Fe$_{1-x}$Co$_x$)$_2$As$_2$ [47], in which superconductivity is induced by hole and electron doping, respectively. In these systems, the existence of an AFM quantum critical point has been suggested, and much attention has been paid to the relationship between quantum critical magnetic fluctuations and superconductivity [48–51]. In this section, we introduce the NMR results on the parent compound BaFe$_2$As$_2$ [21] and review our NMR studies on BaFe$_2$(As$_{1-x}$P$_x$)$_2$ [10,11].

2.3.1. BaFe$_2$As$_2$ [21]

Careful As-NMR measurements on single-crystals of BaFe$_2$As$_2$ were performed by Kitagawa et al. [21]. In the following, their NMR results are introduced.

Fig. 13 shows ^{75}As-NMR spectra at the fixed frequency of 48.41 MHz obtained by sweeping the magnetic field parallel and perpendicular to the c-axis at several different temperatures. The spectra at $T = 141$ K are representative of the paramagnetic phase, while the spectra at the other temperatures belong to the AFM ordered phase. As ^{75}As nuclei have spin 3/2,
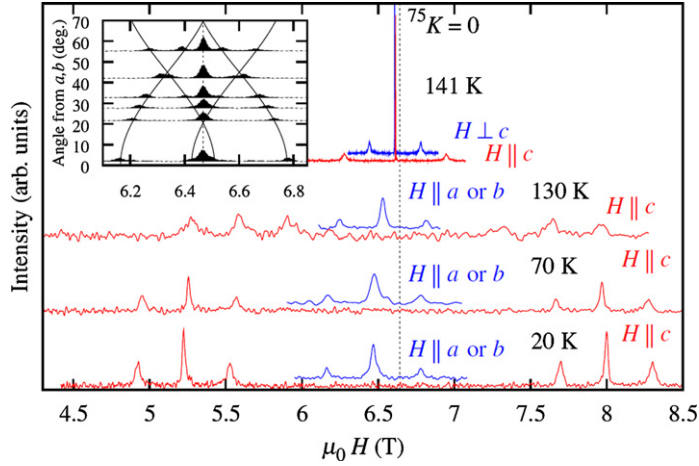
Fig. 13. ^{75}As-NMR spectra obtained by sweeping the magnetic field at the fixed frequency of 48.41 MHz [21]. In the paramagnetic state at 141 K, the spectrum consists of a sharp central line and two broader satellite lines. Below 135 K, the internal fields along the c-axis due to commensurate AFM order splits the NMR spectra for $H \parallel c$ (red lines) and shifts the spectra to lower fields for $H \parallel a$- or b-axis (blue lines). The insert shows the angular variation of the NMR spectrum at 20 K for the field rotated in the ab-plane. The two sets of satellite lines originate from the twinned structural domains in the orthorhombic phase. The satellite positions are fitted to Eq. (2) with the quadrupole parameters; $\nu^c = 2.21$ MHz, $|\nu^a - \nu^b|/\nu^c = 1.18$ (solid lines). Copyright 2008, the Japanese Physical Society.

the NMR frequencies are generally expressed by a perturbation series when the magnetic Zeeman interaction dominates over the quadrupole interaction,

$$\nu_{m \leftrightarrow m-1} = \mu_0 \, {}^{75}\gamma \, H_{\text{eff}} + \frac{1}{2} \nu^c \left(m - \frac{1}{2} \right) \left(3 \cos^2 \theta - 1 + \frac{\nu^a - \nu^b}{\nu^c} \sin^2 \theta \cos 2\phi \right) + (\text{second-order correction}) \tag{2}$$

The first term is the Zeeman frequency, where $^{75}\gamma = 7.29019$ MHz/T is the nuclear gyromagnetic ratio and H_{eff} is the effective field at the As nuclei. In the PM state, the effective field is expressed as $H_{\text{eff}} = (1 + K^i)H$, where H is the external field and K^i is the Knight shift along the i-axis. The second term represents the first-order quadrupolar shift for the three nuclear transitions $I_z = m \leftrightarrow m - 1$ ($m = 3/2, 1/2$, or $1/2$). The explicit expression for the second-order correction can be found in a standard textbook [19]. The quadrupole splitting parameters ν^i ($i = a, b, c$) are related to the electric field gradient (EFG) tensor $V_{\alpha\beta} = \partial^2 V / \partial r_\alpha \, \partial r_\beta$ at the As nuclei as $\nu^i = eV_{ii}Q/2\hbar$, where Q is the nuclear quadrupole moment of ^{75}As. Here the crystal axes are defined with respect to the orthorhombic ($Fmmm$) unit cell. Note that the $mm2$ symmetry of the As sites in the orthorhombic phase guarantees that the crystalline a, b, and c axes are the principal axes of EFG tensor. The polar angle (θ, ϕ) specifies the direction of the magnetic field relative to the crystalline axes. In the tetragonal phase, the NMR spectrum is independent of ϕ since $\nu_a = \nu_b = -\nu_c/2$. As shown in Fig. 13, the NMR spectra at $T = 141$ K show a sharp central line ($m = 1/2$) with the full width at half maximum (FWHM) of 3.5 kHz and two broader satellite lines ($m = 3/2$ and $1/2$) with the FWHM of 100 kHz. The quadrupole splitting ν_c is determined from the separation between the two satellite lines for $H \perp c$ ($\theta = \pi/2$), which is half of the separation for $H \parallel c$ ($\theta = 0$) as expected. The value of ν_c is plotted against temperature in Fig. 14.

When the temperature is lowered below 135 K, the NMR spectrum develops a two-fold splitting for $H \parallel c$. This is the direct evidence for a two-sublattice AFM order. The AFM moments generate a spontaneous internal field with alternating sign $\pm\Delta$, therefore $H_{\text{eff}} = H \pm \Delta$ in Eq. (2). The temperature dependence of Δ determined from the separation between the split center lines is shown in Fig. 15 by crosses. No splitting was observed when the field is applied along the a- or b-axis. Instead, the whole spectrum is shifted to lower fields as seen in Fig. 13. This indicates that the internal field is parallel to the c-axis. When $H \perp c$, H_{eff} is given by the magnitude of the vector sum of the mutually orthogonal external and internal fields, $H_{\text{eff}} = \sqrt{H^2 + \Delta^2}$, giving positively shifted unsplit resonance lines. In Fig. 15, Δ determined also from the shift of the central line for $H \parallel a$ or b is plotted by squares. The values of Δ for the two field orientations show good agreement, indicating that the magnitude and the direction of the AFM moment are independent of the field direction. The behavior in the vicinity of the phase transition was investigated by recording the peak intensity of the Fourier transformed spectrum at the resonance position of the paramagnetic phase with changing temperature as shown in the insert of Fig. 15. The magnetic transition was found to be very sharp with the transition width less than 1 K, indicating good homogeneity of the crystal. It also shows a clear hysteresis in temperature about 4 K wide, providing a conclusive evidence for the first-order transition. This is also inferred from the discontinuous development of the internal field as well as a discontinuous structural transition suggested by a pronounced change of symmetry of EFG. As shown in the insert of Fig. 13, the quadrupole splitting at 20 K varies with the field direction (ϕ) in the ab-plane, indicating that $\nu_a \neq \nu_b$. This is consistent with the orthorhombic symmetry. The angular variation of the NMR spectra displayed in the insert of Fig. 13 shows two branches of satellite lines, which are shifted
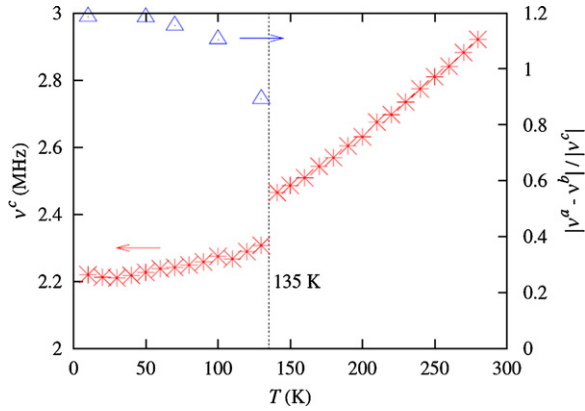
Fig. 14. Nuclear quadrupole splitting frequency along the c-axis, ν_c, and the asymmetry parameter $|\nu_a - \nu_b|/|\nu_c|$ are plotted as a function of temperature [21]. The asymmetry parameter is zero in the tetragonal phase. Its emergence below 135 K and a jump in ν_c indicate the first-order structural transition into the orthorhombic phase. Copyright 2008, the Japanese Physical Society.
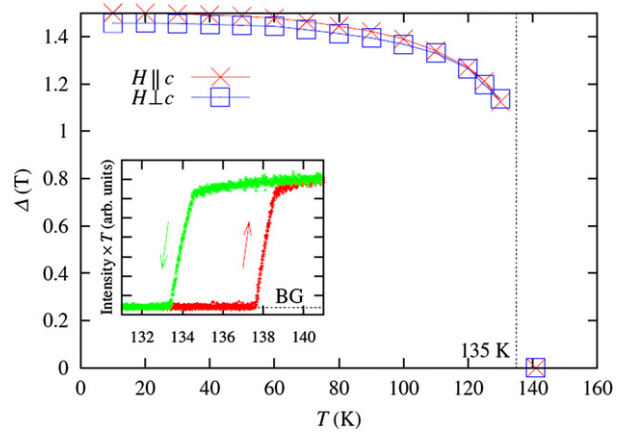

Fig. 15. The temperature dependence of the internal field at the As nuclei associated with the antiferromagnetic order [21]. The insert shows the intensity of the central line at the resonance position of the paramagnetic phase for $H \perp c$. The abrupt change with hysteresis is the evidence for the first-order magnetic transition. Copyright 2008, the Japanese Physical Society.
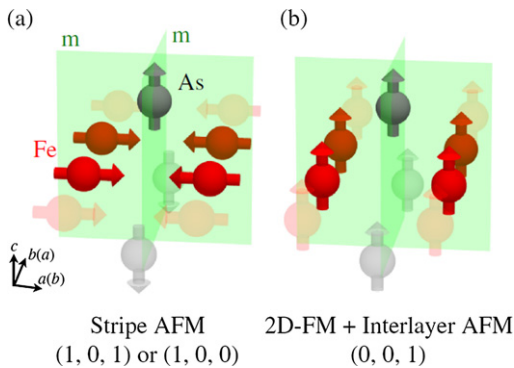

Fig. 16. Possible spin configurations in the AFM ordered state in $BaFe_2As_2$, which is compatible with the ^{75}As-NMR results [21]. Only one Fe–As layer is drawn for simplicity. The internal field at the As sites are shown by grey arrows. There are two candidates: (a) the stripe AFM order and (b) AFM stacking of the ferromagnetic layers. The former case (a) is realized in $BaFe_2As_2$ (see text). Copyright 2008, the Japanese Physical Society.
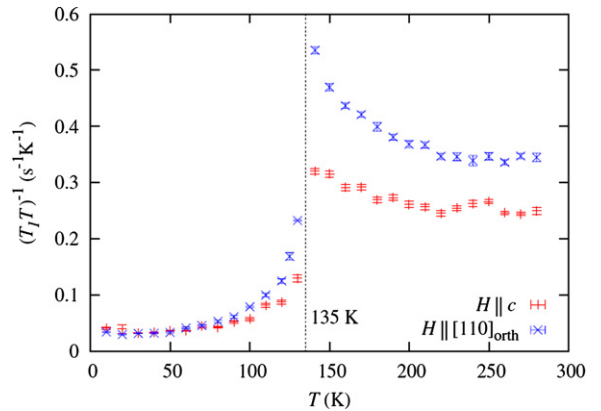

Fig. 17. Nuclear spin-lattice relaxation rate divided by temperature, $1/T_1T$, is plotted as a function of temperature for two field-orientations [21]. The behavior, $T_1T = $ const., at low temperatures indicates the itinerant (Fermi liquid) character of the material. We should remark that the upturn of $1/T_1T$ in the paramagnetic phase is observed only for $H \perp c$. This indicates anisotropic development of the stripe-type antiferromagnetic spin fluctuations perpendicular to both the c-axis and the stripe. Copyright 2008, the Japanese Physical Society.

by 90°. This comes from the twinned orthorhombic domains. The ϕ dependence of the satellite lines can be fit to Eq. (2). The extrema of the angular variation correspond to the field directions parallel to either a- or b-axis. The asymmetry parameter of EFG defined by $|\nu_a - \nu_b|/\nu_c$ is plotted in Fig. 14. The asymmetry parameter, which is zero in the tetragonal phase, is observed to develop abruptly below the transition temperature, and a jump in ν_c is also observed across the transition. These results establish the simultaneous structural and magnetic transition. The large value of asymmetry parameter, exceeding one in the low-temperature phase, implies that the principal axis for the largest EFG changes by 90° across the transition. This suggests that the band structure or the nature of the Fe–As bonds becomes highly anisotropic in the ab-plane.

The ^{75}As-NMR spectra gives the valuable information about the spin structure in the AFM ordered state. There are two major experimental constraints: (i) the internal field at the As sites is parallel to the c-axis; and (ii) the AFM state has a simple two-sublattice structure. There are two possible spin structures compatible with the NMR experiments as shown in Fig. 16, which generate a finite c-component of the internal field. In the first configuration (a), the AFM order is described by the wave vector (101) or (100), forming stripes with the AFM moments directed perpendicular to the stripe. (Note that we cannot distinguish the orthorhombic a- and b-axes by NMR spectra.) In the second configuration (b), ferromagnetic layers in the ab-plane stack antiferromagnetically along the c-axis. The second structure, however, is highly unlikely since the temperature dependence of the susceptibility rules out ferromagnetic correlation.

The spin-lattice relaxation rate divided by temperature $1/T_1T$ is shown in Fig. 17. In the PM phase, $1/T_1T$ shows anisotropic temperature dependence. Substantial enhancement is seen for $H \parallel a$ or b with decreasing temperature, while

$1/T_1T$ is nearly constant for $H \parallel c$. Across the first-order structural/magnetic transition, $1/T_1T$ drops discontinuously by a factor of three. At low temperatures, $1/T_1T$ approaches a constant value for both field orientation expected for a Fermi liquid. This is consistent with the metallic behavior of the resistivity. The low-temperature phase is characterized as an itinerant antiferromagnetic phase. Although the AFM order may be driven by FS nesting, our results demonstrate that the order is commensurate and a sizable density of states at the Fermi level remains down to $T = 0$.

2.3.2. ^{31}P NMR in the normal state of $BaFe_2(As_{1-x}P_x)_2$ [11]

Spin-fluctuation-mediated superconductivity associated with the suppression of the antiferromagnetism is one likely scenario [16], but the identification of the mechanism is far from settled [52,53]. The difficulty in examining the SC mechanism could arise from complexity in the materials that can lead to ambiguous interpretations; e.g., nonuniversal SC gap functions and limited sample quality. It is thus essential to find a suitable model system to examine the mechanism of superconductivity. We have studied isovalent-doped $BaFe_2(As_{1-x}P_x)_2$ within various SC systems possessing the "122" structure, since isovalent P doping is not expected to add carriers [54], and thus $BaFe_2(As_{1-x}P_x)_2$ maintains the compensation condition, i.e. the volume of the hole FSs is equal to that of the electron FSs. Therefore, we consider that $BaFe_2(As_{1-x}P_x)_2$ is an ideal system to investigate relationship between magnetic fluctuations and superconductivity.

We have performed ^{31}P-NMR measurements on $BaFe_2(As_{1-x}P_x)_2$ for $0.2 \leqslant x \leqslant 0.64$ in order to investigate their normal-state spin dynamics. Samples of a mosaic of single crystals were prepared as described elsewhere [54]. The dHvA experiments observed signals in single crystalline samples from the same batch as $x = 0.41$, 0.56, and 0.64, indicating the excellent quality of our samples [55]. The high quality of our samples is also suggested by the sharp SC transitions [54]. ^{31}P-NMR spectra ($^{31}\gamma/2\pi = 17.237$ MHz/T) were obtained by sweeping frequency in a fixed magnetic field of 4.12 T. The Knight shift K was determined with respect to the reference material H_3PO_4. The ^{31}P nuclear spin-lattice relaxation rate $1/T_1$ was determined by fitting the time dependence of spin-echo intensity after saturation of nuclear magnetization to a theoretical $I = 1/2$ curve with a single component of T_1.

Fig. 18 displays ^{31}P-NMR spectra obtained from the $BaFe_2(As_{1-x}P_x)_2$ crystals. Each ^{31}P NMR spectrum consists of a single line, ruling out microscopic inhomogeneity caused by P substitution. K, which measures the effective field at the nucleus produced by electrons, is described as $K = K_{spin} + K_{chem}$; K_{spin} is the spin part of K and is related to the uniform spin susceptibility $\chi(\mathbf{q}) = 0$, which is proportional to DOS at the Fermi energy $N(E_F)$. K_{chem} is the chemical shift, which is unrelated to $\chi(\mathbf{q}) = 0$, and is estimated to be $\sim 0.018\%$ as follows. Since no obvious AFM fluctuations were detected by NMR at high temperatures as seen in Fig. 19, it would be a good approximation to assume that $\sqrt{T_1T}$ is proportional to $N(E_F)$ at high temperatures, i.e. to assume that the usual Korringa relation holds at 270 K. Based on the plot of $\sqrt{T_1T}$ against K at 270 K for different x shown in the insert of Fig. 18, we can estimate K_{chem} as the intercept. The obtained K_{chem} is $0.018 \pm 0.019\%$, indicating that K_{spin} accounts for 86% of the observed Knight shift for $x = 0.33$. Note that this K_{chem} would be a reasonable value, since the chemical shift for ^{31}P in many diamagnetic insulators is of the order of some hundreds of ppm, which is comparable to this K_{chem} [19]. By assuming $K_{spin} \propto \chi(\mathbf{q}) = 0) = \mu_B^2 N(E_F)$, the P-substitution dependence of K_{spin} at 270 K suggests that the change in $N(E_F)$ would be at most 10% for $x \leqslant 0.64$, which is quantitatively consistent with the result of our band calculation discussed below.

Local-density-approximation (LDA) band-structure calculations were performed for non-spin-polarized $BaFe_2As_2$ and $BaFe_2P_2$, using the WIEN2k package in the APW + local orbital basis [56]. In addition, to obtain systematic changes of the electronic band structure for $BaFe_2(As_{1-x}P_x)_2$, Ikeda et al. performed the LDA calculations for three virtual materials with linearly-interpolated $z = z_0(1 - x) + z_1x$; (i) $BaFe_2As_2$ with fixed $(a, c) = (a_0, c_0)$, (ii) $BaFe_2As_2$ with linearly-interpolated $(a, c) = (a_0(1 - x) + a_1x, c_0(1 - x) + c_1x)$, (iii) $BaFe_2P_2$ with fixed $(a, c) = (a_1, c_1)$, where $a_{0,1}$, $c_{0,1}$, and $z_{0,1}$ are the experimental values for the crystallographic parameters of $BaFe_2As_2$ and $BaFe_2P_2$, respectively [54,57]. Fig. 20 shows the P-doping dependence of the density of states at the Fermi level $N(E_F)$ plotted on a per formula unit basis, for cases (i), (ii), and (iii). $N(E_F)$ barely changes for $x < 0.5$, and then decreases for $x > 0.5$. Such behavior is consistent with our Knight shift results.

As shown in Fig. 18(b), K is almost temperature independent for $x \leqslant 0.56$, and that the absolute value of K in the normal state decreases only slightly upon P substitution. These data indicate that P substitution does not produce significant changes in $\chi(\mathbf{q}) = 0)$ and $N(E_F)$. This is in stark contrast to carrier-doped iron-pnictide superconductors; in electron-doped $Ba(Fe_{1-y}Co_y)_2As_2$, the Knight shift data indicate that $N(E_F)$ of non-SC $y = 0.26$ is approximately 50% that of $y = 0.08$ with the maximum T_c of 26 K [49]. Such drastic effects on $N(E_F)$ via electron doping is expected from the characteristic band structure [15,33]; the calculated $N(E_F)$ rapidly changes near E_F with a negative gradient, resulting in a rapid decrease of $N(E_F)$ with electron doping. Large changes in FSs via charge-carrier doping thus necessarily involve dramatic modification in the DOS and FS nesting resulting in changes in spin fluctuations. In addition to possible changes in T_c due to the modification of spin excitation spectrum [49], drastic changes in $N(E_F)$ can also affect severely T_c [58], and the suggested giant magnetoelastic coupling may lead to further suppressions of T_c [59]. Therefore, the decrease in $N(E_F)$ as well as the suppression of spin fluctuations should be taken into account for the interpretation of possible changes in T_c for electron-doped $Ba(Fe_{1-y}Co_y)_2As_2$. In contrast, the nearly unperturbed K_{spin} by isovalent P-doping demonstrates that $BaFe_2(As_{1-x}P_x)_2$ is an ideal model system to test the relevance of spin fluctuations to superconductivity.

Significant low-energy AFM fluctuations are probed near the maximum T_c via $1/T_1$. $1/T_1T$ is described by the wave-vector average of the imaginary part of the dynamical susceptibility $\chi''(\mathbf{q}, \omega_0)$, i.e., $1/T_1T \propto \sum_{\mathbf{q}} |A(\mathbf{q})|^2 \chi''(\mathbf{q}, \omega_0)/\omega_0$, where $A(\mathbf{q})$ represents the hyperfine coupling between ^{31}P nuclear spins and the surrounding electrons, and ω_0 is the NMR frequency. The Korringa law $T_1TK^2 = $ const. generally holds in a Fermi-liquid (FL) state, but is inapplicable to $BaFe_2(As_{1-x}P_x)_2$

(a) BaFe$_2$(As$_{1-x}$P$_x$)$_2$ T = 225 K
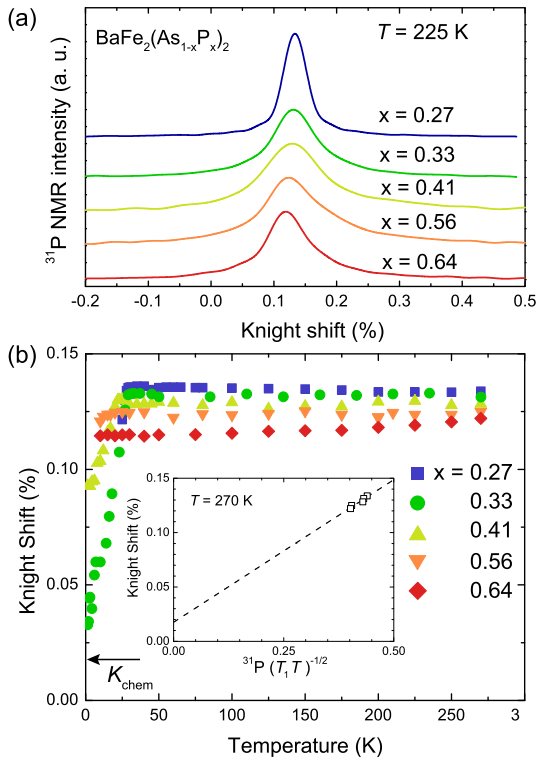
x = 0.27
x = 0.33
x = 0.41
x = 0.56
x = 0.64

Fig. 18. P substitution evolution of (a) ^{31}P-NMR spectra and (b) ^{31}P Knight shift (^{31}K) determined at the spectral peak, obtained in a mosaic of the single crystals at 4.12 T [11]. (b) The arrows indicate the chemical shift K_{chem} (see text). The abrupt decrease in ^{31}K at low temperatures is due to the onset of superconductivity. Inset: ^{31}K vs $(T_1T)^{-1/2}$ at 270 K for different P concentrations x. Copyright 2010, the American Physical Society.

Fig. 19. The ^{31}P nuclear spin-lattice relaxation rate divided by temperature $(T_1T)^{-1}$ for BaFe$_2$(As$_{1-x}$P$_x$)$_2$ at 4.12 T [11]. Solid lines represent fits to $(T_1T)^{-1} = a + b(T+\theta)^{-1}$ (see text). As AFM fluctuations are suppressed as inferred from the suppression of $(T_1T)^{-1}$, T_c (denoted by arrows) also decreases. Inset: Fitting parameters of $(T_1T)^{-1}$. The fitting parameters a and b are plotted against P concentration x. The a and b weakly depend on x, but θ shows a strong x dependence (see Fig. 21). The small value of θ at x = 0.33 ($\theta \sim 0$) are insensitive to the fitting parameters of a and b. Copyright 2010, the America Physical Society.

Fig. 20. Isovalent P-doping dependence of the density of states at the Fermi level $N(E_F)$ plotted on a per formula unit basis, for cases (i), (ii), and (iii) [11]. For this calculation, crystallographic parameters determined experimentally for BaFe$_2$As$_2$ (x = 0) and BaFe$_2$P$_2$ (x = 1) were used. Copyright 2010, the America Physical Society.

near the AFM phase since Curie–Weiss (CW) behavior is observed in $1/T_1T$ (see Fig. 19). For x = 0.33, $1/T_1T$ increases significantly down to T_c whereas the Knight shift is constant. These $1/T_1T$ and K data demonstrate convincingly that AFM fluctuations with finite **q** continue to grow down to T_c at optimal doping.

The AFM fluctuations in BaFe$_2$(As$_{1-x}$P$_x$)$_2$ are enhanced significantly as the P concentration is reduced towards the maximum T_c ($x \simeq 0.33$), as evidenced by the rapid increase in $1/T_1T$ from conventional FL behavior at x = 0.64 (where $1/T_1T$ and K are almost constant). The crossover from FL to CW behavior in $1/T_1T$ correlates perfectly with the change in the resistivity results [54]. As the system evolves from a FL (x = 0.71) towards the maximum T_c (x = 0.33) near the AFM phase, the temperature dependence of the resistivity changes from T^2 to T-linear, one hallmark of non-FL behavior. The exponent of the temperature dependence of the resistivity is shown as a contour plot in Fig. 21(a). Specifically, the CW behavior of $1/T_1T$ and the T-linear resistivity at x = 0.33 can be explained by the existence of two-dimensional (2D) AFM spin fluctuations in the theory of nearly AFM metals [60]. Indeed, the evolution of the AFM spin excitations measured by $1/T_1T$ upon P substitution can be fit consistently by the equation expected from the same theory [60], $1/T_1T = a + b/(T+\theta)$ (see solid lines in Fig. 19). Such 2D AFM fluctuations were experimentally observed in the parent BaFe$_2$As$_2$ via neutron scattering experiments [61]. According to band calculations [62], substantial 2D AFM fluctuations can be generated by the inter-band spin excitations between the multiple FSs predominantly derived from Fe d electrons.
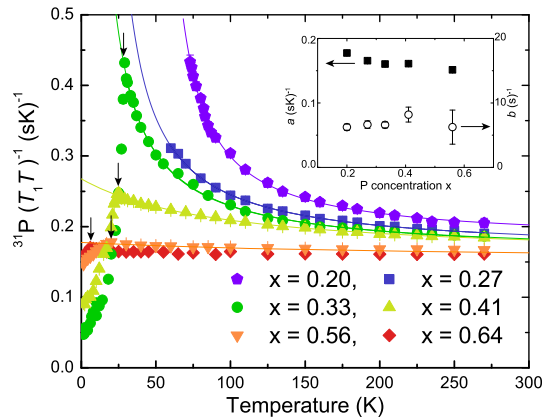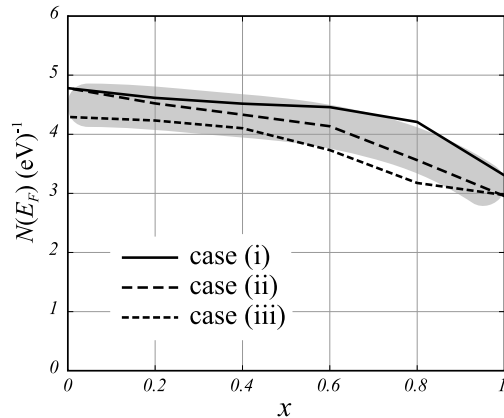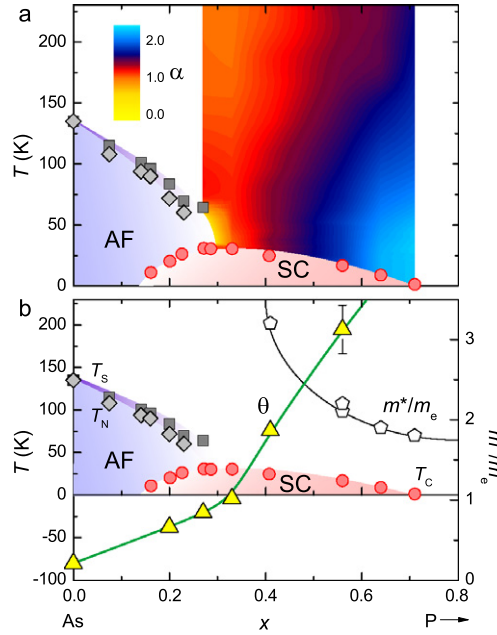
Fig. 21. Temperature–P concentration phase diagram of BaFe$_2$(As$_{1-x}$P$_x$)$_2$ [11]. T_c, T_s, and T_N denote the SC, orthorhombic-tetragonal, and AFM transition temperatures, respectively. (a) Colors represent the exponent, $\alpha = \text{d}(\ln \Delta\rho_{ab})/\text{d}(\ln T)$, at zero magnetic field for the resistivity curves in Ref. [54], where $\Delta\rho_{ab} = \rho_{ab} - \rho_{ab}(T \to 0 \text{ K})$. (b) The triangles represent θ obtained by fitting $(T_1T)^{-1}$ data to the equation, $(T_1T)^{-1} = a + b(T + \theta)^{-1}$ (error bars are within the symbol size). T-linear resistivity, suggesting quantum-critical behavior, is observed in proximity to a magnetic instability signaled by $\theta \simeq 0$ at $x = 0.33$. These quantum-critical fluctuations are found to correlate with the enhancement of the effective mass as denoted by the pentagons (taken from Ref. [55]). Copyright 2010, the America Physical Society.

Our central finding in BaFe$_2$(As$_{1-x}$P$_x$)$_2$ is that the 2D AFM fluctuations of a quantum-critical nature have a clear correlation with the enhancement of quasiparticle effective mass and T_c as summarized in Fig. 21. We found that the Weiss temperature θ obtained from the fitting increases with P substitution and becomes almost zero near $x = 0.33$ where the maximum T_c is achieved. $\theta = 0$ K implies that the dynamical susceptibility probed by $1/T_1T$ measurement diverges at absolute zero, or that the magnetic correlation length continues to increase down to $T = 0$ K. Our result thus strongly suggests the presence of an AFM quantum critical point near the maximum T_c in proximity to the AFM phase boundary. As the P concentration is varied towards optimal doping ($x \sim 0.33$) from $x = 0.64$ where the FL state is observed, the magnetic fluctuations become dramatically enhanced as θ decreases. Importantly, the quasiparticle mass and T_c increase as θ approaches 0 K. This strongly suggests that the AFM quantum-critical fluctuations lead to strong mass renormalization and unconventional superconductivity. Our systematic NMR measurements, which are compared with transport measurements, thus provide the first evidence that the quasiparticle mass enhancement is strongly coupled to the AFM quantum-critical fluctuations in iron-pnictide superconductors as previously observed in heavy fermion systems [63]. Furthermore, since $N(E_F)$ generally correlates with T_c in conventional BCS superconductors, the enhancement of T_c with approaching the quantum critical point from the overdoped side cannot be accounted for by a nearly unperturbed $N(E_F)$, demonstrating clearly that superconductivity in BaFe$_2$(As$_{1-x}$P$_x$)$_2$ is tuned predominantly by the AFM fluctuations. Therefore, we conclude that the 2D AFM quantum-critical fluctuations are likely to play a central role in the occurrence of unconventional superconductivity in BaFe$_2$(As$_{1-x}$P$_x$)$_2$.

Previous NMR measurements also indicated that there is a strong connection between low-energy spin fluctuations and superconductivity in "122" [10], "111" [64–66] and "11" iron-based superconductors [67–70]. These suggest that the relevance of spin fluctuations to the high-T_c superconductivity is universal despite the nonuniversal gap structure. The strong connection would be naturally understood if one considers the superconductivity observed near magnetic phase and the well-nested hole and electron FSs. By contrast, we reported that the connection is relatively weaker in LaFeAs(O$_{1-x}$F$_x$) [7]. Such a weak link may originate from much lower T_c of 26 K in LaFeAs(O$_{1-x}$F$_x$) than that of RFeAs(O$_{1-x}$F$_x$) (R = Ce, Pr, Sm, etc.). However, it remains unresolved whether spin fluctuations are also important for high-T_c superconductivity in the 1111 system with T_c exceeding 50 K, since magnetic rare-earth atoms R hinder quasiparticle excitations responsible for superconductivity [71]. Therefore, examinations of the connection between magnetic fluctuations and superconductivity of high-T_c 1111 iron-pnictides would be crucial for establishing general view of iron pnictide superconductivity.

2.3.3. ^{31}P-NMR in the superconducting state of BaFe$_2$(As$_{1-x}$P$_x$)$_2$ [10]

The SC properties of BaFe$_2$(As$_{0.67}$P$_{0.33}$)$_2$, which is the optimal-doping sample, was investigated with ^{31}P-NMR measurements [10]. We observed a marked $^{31}(1/T_1)$ behavior distinctly different from other iron arsenides. Fig. 22(c) shows that $^{31}(1/T_1)$ decreases sharply just below T_c and there is no evidence for a coherence peak. We find $1/T_1 \propto T$ below ~ 4 K
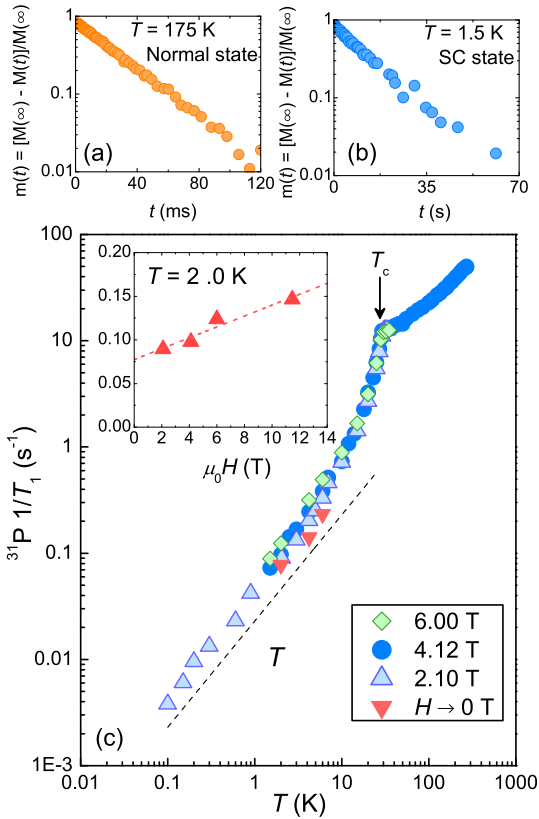
Fig. 22. (a) and (b) show ^{31}P nuclear-spin relaxation curves for 175 and 1.5 K in 4.12 T, exhibiting clear single exponential behavior [10]. (c) ^{31}P $1/T_1$ under 2.1, 4.12, and 6.0 T. Inset in panel (c) shows ^{31}P $1/T_1$ vs magnetic field at 2 K; a linear fit is used to extrapolate $1/T_1$ for $H \to 0$ T. Copyright 2010, the America Physical Society.

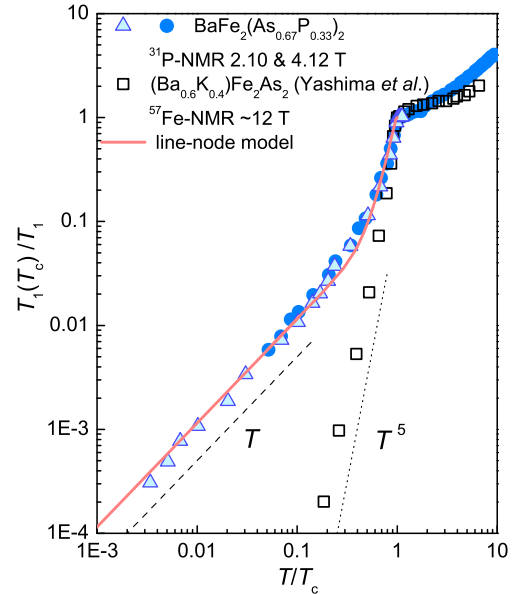**Fig. 23.** Normalized ^{31}P $1/T_1$ for BaFe$_2$(As$_{0.67}$P$_{0.33}$)$_2$ and (Ba$_{0.6}$K$_{0.4}$)Fe$_2$As$_2$ [79]. The solid curve shows a calculation for a line-node gap function $\Delta(\phi) = \Delta_0 \sin(2\phi)$ with $2\Delta_0 = 6k_B T_c$, $N_{res}/N_0 = 0.34$ [10]. Copyright 2010, the America Physical Society.

down to 100 mK, showing the existence of a residual DOS at zero energy. Below about 10 K ($\sim 0.3 T_c$), $1/T_1$ depends on the magnetic field [see Fig. 22(c)]. By extrapolating to zero field, we still find $T_1 T = $ const. behavior below ~ 4 K, excluding the possibility that the $T_1 T = $ const. behavior is attributable to applied fields. The existence of a residual DOS in $H \to 0$ inferred from NMR is consistent with thermal-conductivity results on BaFe$_2$(As$_{0.67}$P$_{0.33}$)$_2$ that reveal a finite thermal conductivity divided by temperature κ_0/T at $T \to 0$ under zero field [62]. Our findings may also be related to the recent specific-heat results on Ba(Fe$_{1-x}$Co$_x$)$_2$As$_2$ [72]. There are two possible contributions to the field dependence of $1/T_1$ arising from quasi-particle excitations in the mixed state: localized quasiparticles inside vortex cores and delocalized quasiparticles originating from nodes in the SC gap. Since the applied fields are much smaller than $H_{c2} \approx 52$ T, localized quasiparticles inside vortex cores are unlikely to contribute to the relaxation at these fields ($H/H_{c2} \leqslant 0.22$). In fact, the thermal-conductivity measurements also show a sizable field dependence of $\kappa_0(H)/T$ at low fields, attaining nearly 70% of the normal-state value even at $0.2 H_{c2}$, indicative of the predominance of delocalized quasiparticles. These results suggest that the field dependence of $1/T_1$ is attributable to the contribution from delocalized quasiparticles originating from nodes in the gap, compatible with the existence of a residual DOS in the SC state. The existence of a residual DOS in the SC state of BaFe$_2$(As$_{0.67}$P$_{0.33}$)$_2$ differs strikingly from other iron arsenides, including "1111" [7,8,20,32,73–76] and "122" superconductors [77–80], instead resembling the cuprates and heavy fermion superconductors, which have nodes in their SC gap.

As shown in Fig. 23, $1/T_1$ of ^{57}Fe in Ba$_{0.6}$K$_{0.4}$Fe$_2$As$_2$ near optimal doping exhibits a T^5-like dependence well below T_c [79]. The fairly large exponent of 5 in $1/T_1$ can be understood by a fully gapped state in Ba$_{0.6}$K$_{0.4}$Fe$_2$As$_2$, and was analyzed in terms of $s_\pm$-wave superconductivity with two gaps [79]. In the $s_\pm$ models with unitary scatterings, in-gap states at zero energy can be induced without severely reducing T_c and can in principle account for the $1/T_1 \propto T$ behavior. However, the penetration depth $\Delta\lambda(T) \propto T$ at low temperatures observed in BaFe$_2$(As$_{0.67}$P$_{0.33}$)$_2$ is incompatible with these models, but is consistent with line nodes in the gap. In a symmetry-imposed nodal superconductor such as described by a linenode model $\Delta = \Delta_0 \sin(2\phi)$, $1/T_1 \propto T^3$ in the clean limit, but impurity scattering induced near gap nodes gives rise to an enhanced $1/T_1$ that is proportional to temperature at low temperatures. P dopants in BaFe$_2$(As$_{0.67}$P$_{0.33}$)$_2$ can provide a source for nonmagnetic scatterers, consistent with the existence of Fermi-level DOS. In fact, the $1/T_1$ data of BaFe$_2$(As$_{0.67}$P$_{0.33}$)$_2$ are well fit by the line-node model with $2\Delta_0/k_B T_c = 6$ and $N_{res}/N_0 = 0.34$, where N_{res}/N_0 is the ratio of a residual DOS in the SC state to that in the normal state (see Fig. 23). Therefore, NMR, penetration-depth, and thermal conductivity results on

$BaFe_2(As_{0.67}P_{0.33})_2$ are consistent with the existence of line nodes in the SC gap. In the case of nodes imposed by symmetry, a residual DOS at zero energy is a natural consequence of the impurity scattering that broadens the nodes. However, this is not clear for the case of "accidental" nodes not imposed by symmetry, as in the extended *s*-wave case because impurity scattering will lift the nodes and produce a more isotropic gap [81]. Our experimental findings impose significant constraints on candidate theoretical descriptions of iron pnictide superconductivity. The strikingly different behavior of $1/T_1$ in the SC state between $BaFe_2(As_{0.67}P_{0.33})_2$ and $Ba_{0.6}K_{0.4}Fe_2As_2$ is surprising because they have comparable T_c values and similar Fermi surfaces. This implies that high-T_c superconductivities with and without nodes are nearly degenerate and that subtle differences can significantly modify the nature of superconductivity [17,82,81,83,84]. Changes in the pnictogen height may lead to nodal superconductivity, but its T_c should be much lower than that of fully gapped $s_\pm$ states [82]. However, this is not the case in $BaFe_2(As_{0.67}P_{0.33})_2$. One notable difference inferred from band calculations [54,62] is that $BaFe_2(As_{0.67}P_{0.33})_2$ may be more three-dimensional than $Ba_{0.6}K_{0.4}Fe_2As_2$, suggesting that a three-dimensional model is required. Reconciling their comparable T_c values and fundamentally different SC gap functions needs further theoretical and experimental works. To clarify this problem, identifying the location of the node on Fermi surfaces will be crucial. In order to know how the SC gap evolves with the P-doping, we have systematically measured $1/T_1$ in the SC state on ther samples with various P concentration.

3. Summary

We have shown NMR results obtained in $LaFeAs(O_{1-x}F_x)$ and $BaFe_2(As_{1-x}P_x)_2$. The following results have been obtained:

1. Undoped LaFeAsO shows AFM ordering at $T_N \sim 142$ K, ~ 15 K below the structural transition T_S. Since AFM fluctuations are enhanced below T_S, the magnetic transition is intimately coupled with the structural transition. On the other hand, two transitions occur simultaneously with a first-order character in $BaFe_2As_2$. The antiferromagnetic *q* vectors, which are $(\pi, 0)$ and $(0, \pi)$ in the "*unfolded*" Brillouin zone and thus correspond to a stripe-type magnetic structure, are suggested also from the analyses of the ^{75}As-NMR spectrum.

2. From the F-concentration and temperature dependence of $1/T_1T$, the low-energy magnetic fluctuations are strongly suppressed by electron doping, and the pseudogap behavior is observed in $1/T_1T$ for $LaFeAs(O_{1-x}F_x)$ and $LaFeAsO_{1-\delta}$ with the maximum T_c. The pseudogap behavior becomes pronounced with F (electron)-doping. The doping dependence of the pseudogap behavior is opposite to that observed in the cuprate superconductors, in which the pseudogap behavior is significant in the underdoped region. The pseudogap behavior is not ascribed to the AFM correlations discussed in the cuprate, but to the character of the band structure near E_F in the iron-pnictide superconductors.

3. $1/T_1T$ in $LaFeAs(O_{1-x}F_x)$ depends significantly on the F-concentration, whereas T_c is insensitive to *x* within a range from $x = 0.04$ to 0.14. Almost constant value of T_c against the F-concentration, irrelevant to the drastic change of $1/T_1T$ in the normal state, suggests that the spin fluctuations observed through the $1/T_1$ measurements do not play a vital role for the superconductivity.

4. In contrast with $LaFeAs(O_{1-x}F_x)$, the ^{31}P-NMR measurements on $BaFe_2(As_{1-x}P_x)_2$ with various P-doping reveal that two-dimensional AFM fluctuations are notably enhanced with little change in static susceptibility on approaching the AFM phase from the SC dome, and that magnetically ordered temperature θ deduced from $1/T_1T$ vanishes at optimal doping. These results strongly indicate the presence of the quantum critical points, and suggest that the AFM fluctuations with the quantum critical character play a central role in the high-T_c superconductivity. Therefore, we suggest that $BaFe_2(As_{1-x}P_x)_2$ shares the commonality with heavy-fermion superconductors which are also in the proximity of magnetic ground states.

5. The relationship between superconductivity and magnetic fluctuations probed with NMR measurement is quite different between $LaFeAs(O_{1-x}F_x)$ and $BaFe_2(As_{1-x}P_x)_2$. The difference of the relationship is also suggested from phase diagrams of two systems [see in Figs. 9 and 21]. (The AFM phase disappears abruptly, and the SC phase with nearly constant T_c appears in $LaFeAs(O_{1-x}F_x)$, but T_N is gradually suppressed by P-doping, and the SC phase appears as if it covers the magnetic quantum critical point in $BaFe_2(As_{1-x}P_x)_2$). However, since the $1/T_1$ measurements can detect the low-energy magnetic fluctuations (typically $\sim$ mK order), and might fail to detect important magnetic fluctuations if their characteristic energy exceeds the limitation of the NMR experiments, the inelastic neutron experiments over wide *q*-space and energy range are needed for uncovering magnetic fluctuations thoroughly, particularly on "1111" compounds.

6. $1/T_1$ in the SC state on $LaFeAs(O_{1-x}F_x)$ shows the absence of a coherence peak just below T_c and the T^3 temperature dependence down to $\sim 0.2T_c$. The T^3 dependence in the compounds suggests highly anisotropic superconducting gaps with gap-zero regions along lines, whereas the absences of the field-induced extra relaxation rate and of the residual DOS at low temperatures are incompatible with *d*-wave superconductivity. The absence of the coherence peak in $1/T_1$ just below T_c is interpreted in terms of the $s_\pm$-wave model.

7. $1/T_1$ result in the SC state on $BaFe_2(As_{0.67}P_{0.33})_2$ shows the existence of a residual DOS at zero energy, which is consistent with the presence of nodes in the SC gap inferred from a field dependence of $1/T_1$ and from thermal conductivity and penetration-depth results. This suggests that strikingly different SC gaps appear in $BaFe_2(As_{1-x}P_x)_2$ despite comparable high-T_c values, analogous phase diagrams, and similar FSs with $(Ba_{1-x}K_x)Fe_2As_2$.

Acknowledgements

References

[1] Y. Kamihara, T. Watanabe, M. Hirano, H. Hosono, J. Am. Chem. Soc. 130 (2008) 3296.
[2] H. Takahashi, K. Igawa, K. Arii, Y. Kamihara, M. Hirano, H. Hosono, Nature 453 (2008) 376.
[3] C. Wang, L. Li, S. Chi, Z. Zhu, Z. Ren, Y. Li, Y. Wang, X. Lin, Y. Luo, S. Jiang, X. Xu, G. Cao, Z. Xu, Europhys. Lett. 83 (2008) 67006.
[4] Z.-A. Ren, W. Lu, J. Yang, W. Yi, X.-L. Shen, Z.-C. Li, G.-C. Che, X.-L. Dong, L.-L. Sun, F. Zhou, Z.-X. Zhao, Chin. Phys. Lett. 25 (2008) 2215.
[5] H. Kito, H. Eisaki, A. Iyo, J. Phys. Soc. Jpn. 77 (2008) 063707.
[6] Z.-A. Ren, G.-C. Che, X.-L. Dong, J. Yang, W. Lu, W. Yi, X.-L. Shen, Z.-C. Li, L.-L. Sun, F. Zhou, Z.-X. Zhao, EPL 83 (2008) 17002.
[7] Y. Nakai, K. Ishida, Y. Kamihara, M. Hirano, H. Hosono, J. Phys. Soc. Jpn. 77 (2008) 073701.
[8] Y. Nakai, S. Kitagawa, K. Ishida, Y. Kamihara, M. Hirano, H. Hosono, New J. Phys. 11 (2009) 045004.
[9] K. Ishida, Y. Nakai, H. Hosono, J. Phys. Soc. Jpn. 78 (2009) 062001.
[10] Y. Nakai, T. Iye, S. Kitagawa, K. Ishida, Y.M.S. Kasahara, T. Shibauchi, T. Terashima, Phys. Rev. B 81 (2010) 020503(R).
[11] Y. Nakai, T. Iye, S. Kitagawa, K. Ishida, H. Ikeda, S. Kasahara, H. Shishido, T. Shibauchi, Y. Matsuda, T. Terashima, Phys. Rev. Lett. 105 (2010) 107003.
[12] C. de la Cruz, Q. Huang, J.W. Lynn, J. Li, W. Ratcliff II, J.L. Zarestky, H.A. Mook, G.F. Chen, J.L. Luo, N.L. Wang, P. Dai, Nature 453 (2008) 899.
[13] T. Nomura, S.W. Kim, Y. Kamihara, M. Hirano, P.V. Sushko, K. Kato, M. Takata, A.L. Shluger, H. Hosono, Supercond. Sci. Technol. 21 (2008) 125028.
[14] L. Boeri, O.V. Dolgov, A.A. Golubov, Phys. Rev. Lett. 101 (2008) 026403.
[15] D.J. Singh, M.H. Du, Phys. Rev. Lett. 101 (2008) 237003.
[16] I.I. Mazin, D.J. Singh, M.D. Johannes, M.H. Du, Phys. Rev. Lett. 101 (2008) 057003.
[17] K. Kuroki, S. Onari, R. Arita, H. Usui, Y. Tanaka, H. Kontani, H. Aoki, Phys. Rev. Lett. 101 (2008) 087004.
[18] A. Cox, M.J.L. Sangster, J. Phys. C: Solid State Phys. 18 (1985) L1123.
[19] G.C. Carter, L.H. Bennett, D.J. Kahan, Metallic Shifts in NMR, Prog. Mater. Sci., vol. 20, Pergamon, Oxford, 1977.
[20] H. Mukuda, N. Terasaki, H. Kinouchi, M. Yashima, Y. Kitaoka, S. Suzuki, S. Miyasaka, S. Tajima, K. Miyazawa, P. Shirage, H. Kito, H. Eisaki, A. Iyo, J. Phys. Soc. Jpn. 77 (2008) 093704.
[21] K. Kitagawa, N. Katayama, K. Ohgushi, M. Yoshida, M. Takigawa, J. Phys. Soc. Jpn. 77 (2008) 114709.
[22] S.H. Baek, T. Klimczuk, F. Ronning, E.D. Bauer, N.J. Curro, J.D. Thompson, Phys. Rev. B 78 (2008) 212509.
[23] D.E. MacLaughlin, J.P. Vithayathil, H.B. Brom, J.C.J.M. de Rooy, P.C. Hammel, P.C. Canfield, A.P. Reyes, Z. Fisk, J.D. Thompson, S.-W. Cheong, Phys. Rev. Lett. 72 (1994) 760.
[24] T. Moriya, Spin Fluctuations in Itinerant Electron Magnetism, Springer-Verlag, 1985.
[25] Y. Kitaoka, Yasuoka, J. Phys. Soc. Jpn. 48 (1980) 1460.
[26] S.H. Baek, N.J. Curro, T. Klimczuk, E.D. Bauer, F. Ronning, J.D. Thompson, arXiv:0808.0744, 2008.
[27] T. Nakano, N. Fujiwara, Y. Kamihara, M. Hirano, H. Hosono, H. Okada, H. Takahashi, Phys. Rev. B 82 (2010) 172502.
[28] R. Klingeler, N. Leps, I. Hellmann, A. Popa, C. Hess, A. Kondra, J. Hamann-Borrero, G. Behr, V. Kataev, B. Buechner, Phys. Rev. B 81 (2010) 024506.
[29] M. Takigawa, A.P. Reyes, P.C. Hammel, J.D. Thompson, R. Heffner, Z. Fisk, K.C. Ott, Phys. Rev. B 43 (1991) 247.
[30] T. Imai, K. Ahilan, F. Ning, M.A. McGuire, A.S. Sefat, R. Jin, B.C. Sales, D. Mandrus, J. Phys. Soc. Jpn. (Suppl. C) 77 (2008) 47.
[31] S. Takeshita, R. Kadono, M. Hiraishi, M. Miyazaki, A. Koda, Y. Kamihara, H. Hosono, J. Phys. Soc. Jpn. 77 (2008) 103703.
[32] N. Terasaki, H. Mukuda, M. Yashima, Y. Kitaoka, K. Miyazawa, P.M. Shirage, H. Kito, H. Eisaki, A. Iyo, J. Phys. Soc. Jpn. 78 (2009) 013701.
[33] H. Ikeda, J. Phys. Soc. Jpn. 77 (2008) 123707.
[34] G.-q. Zheng, H. Ozaki, Y. Kitaoka, P. Kuhns, A.P. Reyes, W.G. Moulton, Phys. Rev. Lett. 88 (2002) 077003.
[35] K. Ishida, H. Mukuda, Y. Kitaoka, Z.Q. Mao, Y. Mori, Y. Maeno, Phys. Rev. Lett. 84 (2000) 5387.
[36] N.J. Curro, T. Calwell, E.D. Bauer, L.A. Morales, M.J. Graf, Y. Bang, A.V. Balatsky, J.D. Thompson, J.L. Sarrao, Nature 434 (2005) 622.
[37] H. Ding, P. Richard, K. Nakayama, K. Sugawara, T. Arakane, Y. Sekiba, A. Takayama, S. Souma, T. Sato, T. Takahashi, Z. Wang, X. Dai, Z. Fang, G.F. Chen, J.L. Luo, N.L. Wang, Europhys. Lett. 83 (2008) 47001.
[38] K. Hashimoto, T. Shibauchi, T. Kato, K. Ikada, R. Okazaki, H. Shishido, M. Ishikado, H. Kito, A. Iyo, H. Eisaki, S. Shamoto, Y. Matsuda, Phys. Rev. Lett. 102 (2009) 017002.
[39] L.S. Borkowski, P.J. Hirschfeld, Phys. Rev. B 49 (1994) 15404.
[40] D. Parker, O.V. Dolgov, M.M. Korshunov, A.A. Golubov, I.I. Mazin, Phys. Rev. B 78 (2008) 134524.
[41] A.V. Chubukov, D.V. Efremov, I. Eremin, Phys. Rev. B 78 (2008) 134512.
[42] M.M. Parish, J. Hu, B.A. Bernevig, Phys. Rev. B 78 (2008) 144514.
[43] Y. Nagai, N. Hayashi, N. Nakai, H. Nakamura, M. Okumura, M. Machida, New J. Phys. 10 (2008) 103026.
[44] S. Kawasaki, T. Mito, Y. Kawasaki, G.q. Zheng, Y. Kitaoka, D. Aoki, Y. Haga, Y. Ōnuki, Phys. Rev. Lett. 91 (2003) 137001.
[45] K. Haule, J.H. Shim, G. Kotliar, Phys. Rev. Lett. 100 (2008) 226402.
[46] M. Rotter, M. Tegel, D. Johrendt, Phys. Rev. Lett. 101 (2008) 107006.
[47] A.S. Sefat, R. Jin, M.A. McGuire, B.C. Sales, D.J. Singh, D. Mandrus, Phys. Rev. Lett. 101 (2008) 117004.
[48] J.H. Chu, J.G. Analytis, C. Kucharczyk, I.R. Fisher, Phys. Rev. B 79 (2008) 014506.
[49] F.L. Ning, K. Ahilan, T. Imai, A.S. Sefat, M.A. McGuire, B.C. Sales, D. Mandrus, P. Cheng, B. Shen, H.H. Wen, Phys. Rev. Lett. 104 (2010) 017204.
[50] C. de la Cruz, W.Z. Hu, S. Li, Q. Huang, J.W. Lynn, M.A. Green, G.F. Chen, N.L. Wang, H.A. Mook, Q. Si, P. Dai, Phys. Rev. Lett. 104 (2010) 017204.
[51] J. Dai, Q. Si, J.X. Zhu, E. Abrahams, Proc. Natl. Acad. Sci. USA 106 (2009) 4118.
[52] H. Kontani, S. Onari, Phys. Rev. Lett. 104 (2010) 157001.
[53] I. Mazin, J. Schmalian, Physica C (Amsterdam) 469 (2009) 614.
[54] S. Kasahara, T. Shibauchi, K. Hashimoto, K. Ikada, S. Tonegawa, R. Okazaki, H. Shishido, H. Ikeda, H. Takeya, K. Hirata, T. Terashima, Y. Matsuda, Phys. Rev. B 81 (2010) 184519.

[55] H. Shishido, A.F. Bangura, A.I. Coldea, S. Tonegawa, K. Hashimoto, S. Kasahara, P.M.C. Rourke, H. Ikeda, T. Terashima, R. Settai, Y. Ōnuki, D. Vignolles, C. Proust, B. Vignolle, A. McCollam, Y. Matsuda, T.S.A. Carrington, Phys. Rev. Lett. 104 (2010) 057008.
[56] P. Blaha, K. Schwarz, G.K.H. Madsen, D. Kvasnicka, J. Luitz, in: K. Schwarz (Ed.), An Augmented Plane Wave Plus Local Orbitals Program for Calculating Crystal Properties, Techn. Universitat Wien, Austria, 2001.
[57] M. Rotter, M. Tegel, D. Johrendt, Phys. Rev. B 78 (2008) 020503(R).
[58] E.Z. Kuchinskii, I.A. Nekrasov, M.V. Sadovskii, arXiv:1004.0801, 2010.
[59] T. Yildirim, Physica C (Amsterdam) 469 (2009) 425.
[60] T. Moriya, Y. Takahashi, K. Ueda, J. Phys. Soc. Jpn. 59 (1990) 2905.
[61] K. Matan, R. Morinaga, K. Iida, T.J. Sato, Phys. Rev. B 79 (2009) 054526.
[62] K. Hashimoto, M. Yamashita, S. Kasahara, Y. Senshu, N. Nakata, S. Tonegawa, K. Ikada, A. Serafin, A. Carrington, T. Terashima, H. Ikeda, T. Shibauchi, Y. Matsuda, Phys. Rev. B 81 (2010) 220501.
[63] H. Shishido, R. Settai, H. Harima, Y. Ōnuki, J. Phys. Soc. Jpn. 74 (2005) 1103.
[64] L. Ma, J. Zhang, D.M. Wang, J.B. He, T.-L. Xia, G.F. Chen, W. Yu, arXiv:1005.1448, 2010.
[65] P. Jeglič, A. Potočnik, M. Klanjšek, M. Bobnar, M. Jagodič, K. Koch, H. Rosner, S. Margadonna, B. Lv, A.M. Guloy, D. Arčon, Phys. Rev. B 81 (2010) 140511.
[66] Z. Li, Y. Ooe, X.-C. Wang, Q.-Q. Liu, C.-Q. Jin, M. Ichioka, G.q. Zheng, J. Phys. Soc. Jpn. 79 (2010) 083702.
[67] T. Imai, K. Ahilan, F.L. Ning, T.M. McQueen, R.J. Cava, Phys. Rev. Lett. 102 (2009) 177005.
[68] S. Masaki, H. Kotegawa, Y. Hara, H. Tou, K. Murata, Y. Mizuguchi, Y. Takano, J. Phys. Soc. Jpn. 78 (2009) 063704.
[69] Y. Shimizu, T. Yamada, T. Takami, S. Niitaka, H. Takagi, M. Itoh, J. Phys. Soc. Jpn. 78 (2009) 123709.
[70] C. Michioka, H. Ohta, M. Matsui, J. Yang, K. Yoshimura, M. Fang, Phys. Rev. B 82 (2010) 064506.
[71] H. Yamashita, M. Yashima, H. Mukuda, Y. Kitaoka, P.M. Shirage, A. Iyo, Physica C (Amsterdam) (2009), doi:10.1016.
[72] G. Mu, B. Zeng, P. Cheng, Z. Wang, L. Fang, B. Shen, L. Shan, C. Ren, H. Wen, Chin. Phys. Lett. 27 (2010) 037402.
[73] H.-J. Grafe, D. Paar, G. Lang, N.J. Curro, G. Behr, J. Werner, J. Hamann-Borrero, C. Hess, N. Leps, R. Klingeler, B. Büchner, Phys. Rev. Lett. 101 (2008) 047003.
[74] K. Matano, Z.A. Ren, X.L. Dong, L.L. Sun, Z.X. Zhao, G.q. Zheng, Europhys. Lett. 83 (2008) 57001.
[75] S. Kawasaki, K. Shimada, G.F. Chen, J.L. Luo, N.L. Wang, G.q. Zheng, Phys. Rev. B 78 (2008) 220506(R).
[76] Y. Kobayashi, A. Kawabata, S.C. Lee, T. Moyoshi, M. Sato, J. Phys. Soc. Jpn. 78 (2009) 073704.
[77] H. Fukazawa, T. Yamazaki, K. Kondo, Y. Kohori, N. Takeshita, P.M. Shirage, K. Kihou, K. Miyazawa, H. Kito, H. Eisaki, A. Iyo, J. Phys. Soc. Jpn. 78 (2009) 033704.
[78] K. Matano, G.L. Sun, D.L. Sun, C.T. Lin, M. Ichioka, G.Q. Zheng, Europhys. Lett. 87 (2009) 27012.
[79] M. Yashima, H. Nishimura, H. Mukuda, Y. Kitaoka, K. Miyazawa, P.M. Shirage, K. Kihou, H. Kito, H. Eisaki, A. Iyo, J. Phys. Soc. Jpn. 78 (2009) 103702.
[80] H. Fukazawa, Y. Yamada, K. Kondo, T. Saito, Y. Kohori, K. Kuga, Y. Matsumoto, S. Nakatsuji, H. Kito, P.M. Shirage, K. Kihou, N. Takeshita, C.H. Lee, A. Iyo, H. Eisaki, J. Phys. Soc. Jpn. 78 (2009) 083712.
[81] V. Mishra, G. Boyd, S. Graser, T. Maier, P.J. Hirschfeld, D.J. Scalapino, Phys. Rev. B 79 (2009) 094512.
[82] K. Kuroki, H. Usui, S. Onari, R. Arita, H. Aoki, Phys. Rev. B 79 (2009) 224511.
[83] K. Seo, B.A. Bernevig, J. Hu, Phys. Rev. Lett. 101 (2008) 206404.
[84] A.V. Chubukov, M.G. Vavilov, A.B. Vorontsov, Phys. Rev. B 80 (2009) 140515.